UNIVERSITY OF CALIFORNIA,
IRVINE

Quantification of Downtime in a Highway Network during Seismic Events

THESIS

submitted in partial satisfaction of the requirements
for the degree of

MASTER OF SCIENCE

in Civil Engineering

by

Preetish Kakoty

Thesis Committee:
Associate Professor Farzin Zareian, Chair
Adjunct Professor Farzad Naeim
Professor Lizhi Sun

2017

TABEL OF CONTENTS

LIST OF FIGURES

LIST OF TABLES

ACKNOWLEDGEMENT

I would like to take this opportunity to thank my advisor Professor Farzin Zareian for his continuous guidance and support throughout my MS at the University of California, Irvine. He has been very kind to provide technical support as well as boosting confidence from time to time. I will always cherish the time I have spent with him through numerous research meetings and the role he has played in my development as a researcher and a student. I offer my sincere gratitude towards him and feel very fortunate to have worked with him for my MS thesis.

I would also like to thank Dr. Farzad Naeim and Professor Lizhi Sun, members of my thesis committee for providing valuable advice whenever I needed them. I thank professor Wenlong Jin and Dr. Qijian Gan of Institute of Transportation Studies, UC Irvine for providing their expertise and sharing the traffic data which is a very crucial part of the work. I would also like to thank Lisa Preble of the Engineering Computing Trailer for helping me in carrying out the simulations in the computing facility.

The discussions in the Performance Based Earthquake Engineering Laboratory with my fellow students have encouraged me and helped me go through the ups and downs during this journey. I would like to thank and appreciate Rachelle, Jim, Pablo, Shayan, Behzad and Marta for their support and comradery.

I would also like to thank my friends in UC Irvine as well as back home in India for always being there whenever I needed anything.

And last, but certainly not least, I would like to thank my family. Although living thousands of miles away, they have always been the pillar of strength and confidence for me. Their mental support and believe in me has always kept me going.

ABSTRACT

Quantification of Downtime in a Highway Network during Seismic Events

By

Preetish Kakoty

Master of Science in Civil Engineering

University of California, Irvine, 2017

Associate Professor Farzin Zareian, Chair

This study aims at quantifying the losses occurring in a highway network due to low ground motion intensities which causes non-structural damage resulting in short duration of bridge closure. In a highway network, the bridges are the most vulnerable elements and structural damage on the bridges give rise to a huge amount of economic loss due to repair and downtime. Research efforts were put to quantify these losses for large earthquakes causing the bridges to close for long period of time. Estimating the impact of low ground motion intensity that do not cause any structural damage rather short duration of disruption owing to non-structural damage and inspection is investigated in this study. The focus is on quantifying short downtime of bridges in terms of economic losses and assessing the impact these events have in the broad picture.

The study involves probabilistic seismic hazard analysis at the bridge sites of the SR-91 highway network and create earthquake scenarios and concurrently conduct traffic simulation to estimate the delay in the network. The traffic simulations are carried out in TransModeller for different scenarios considering two durations of bridge closure: half-hour and two-hour. The delay in the network is converted to monetary loss as per the cost analysis parameters by Caltrans. The economic loss for the specific cases of ground motion lies in the range of $1.5 million to $4.5 million with a 15-year return period.

CHAPTER 1

INTRODUCTION

1.1.Motivation and Objective

Infrastructure systems are very important for the proper functioning of a society and hence they are often referred to as lifeline systems. Disruption in lifeline systems can majorly impact the social and economic activities of a society. The infrastructure systems add a layer of complexity for seismic analysis because of the spatial distribution. Seismic risk analysis of the infrastructure system is very important to understand and mitigate the risk associated with it. Seismic risk analysis gives the annual probability of exceedance of certain losses during future earthquakes. This information about economic losses is important for decision makers to manage and mitigate risk efficiently. Transportation network is one of the most important infrastructure system for any community and this work is focused on quantifying the losses in a transportation network due to seismic events. Disruption in transportation network can implicate huge business losses in terms of economy and opportunity; for instance there was more than $1.5 billion loss in business interruption because of damage in transportation network during the Northridge earthquake [Chang, 2003]. There have been efforts to quantify the losses in a transportation network previously, creating and adapting state-of-the-art methodologies to carry out risk analysis of complex transportation networks for seismic events [Werner et al.,2000; Moore et al.,1997; Banerjee and Shinozuka, 2008; Jayaram and Baker, 2010; REDARS 2006]. Most of the research efforts have been directed towards quantifying the losses in a transportation network for major damage in the system.

In a transportation network, the bridges are the most vulnerable elements. There are major disruptions in traffic flow when a major earthquake strikes and damages the bridges and this results in massive economic losses. In a seismically active region like California, there are concerns over the possible losses for any level of hazards and efforts have to be put into minimizing the risk. Therefore, this research aims

to look at the possible risk because of the low to moderate level of ground motions which do not result into structural damage of the bridges but closure of the bridges for a short period of time. Even short period of closure in bridges can affect the functioning of a transportation network and increase the travel time significantly causing major economic loss due to business interruption. The research is directed towards getting an insight into the effects of short closure of bridges because of moderate ground motion intensity on economy. Essentially, the research comprises of three major tasks: carrying out a probabilistic seismic hazard analysis (PSHA) for the transportation network, performing a traffic simulation with different scenarios of transportation network closure, and quantifying the downtime in terms of the economic losses incurred in all the earthquake scenarios considered during the PSHA.

Traditionally, the PEER framework has been applied for loss estimation of a single structure at a given site [Cornell and Krawlinker, 2000; Deierlein, 2004]. The risk analysis is performed to obtain the exceedance of various loss levels, computed as follows:

$$\lambda(DV) = \iiint G(DV|DM)dG(DM|EDP)dG(EDP|IM)|d\lambda(IM)|$$

Where, $\lambda(DV)$ is the exceedance rate of the decision variable which in this case is the loss level, $d\lambda(IM)$ is the exceedance rate of the ground motion intensity measure. $dG(DM|EDP)$ represents the derivative of the probability of exceedance of damage measure (DM) given the engineering demand parameter (EDP). Similarly, $dG(EDP|IM)$ represents the derivative of the probability of exceedance of EDP given the ground motion intensity measure. And, $G(DV|DM)$ represents the probability of exceedance of decision variable given the damage measure. In case of a single structure, numerical integration is carried out to calculate the exceedance of loss level. But the estimation of exceedance rate of loss level for an infrastructure system is much complicated in this framework because it involves a large vector of ground motion intensity (IM) and also because most of the probability relations are not available in closed form. There is also significant spatial correlation between the parameters in the infrastructure system. Alternatively, researchers have used analytical approaches for risk analysis of transportation network problems [Kang et al., 2008]. The most

popular approach in this regard has been the Monte-Carlo simulation procedure and researchers have utilized Monte-Carlo simulation for risk analysis problems, for example Chang et al.,2000; Werner et al., 2004; Crowley and Bommer, 2006; Kiremidjian et al.,2007; Jayaram and Baker, 2010 etc. This research also uses Monte-Carlo simulation to carry out the risk analysis of the transportation network for seismic events.

The risk analysis is proposed to be conducted over the SR-91 highway in California, which runs through Los Angeles, Orange and Riverside counties. Here, the section of highway falling in the Orange County is being considered. In Orange County, SR-91 connects the Los Angeles county line to the Riverside county line. The corridor is approximately 25 miles long and consist of 10 bridges. This corridor of SR-91 passes through Anaheim, Fullerton, Placentia, and Yorba Linda and includes four major freeway-to-freeway interchanges: I-5, SR-57, SR-55, and the SR-241 Eastern Transportation Corridor Toll Road [CSMP SR-91, 2010]. Caltrans traffic volumes in 2008 reported that the annual average daily traffic in this corridor of SR-91 lies between 217,000 and 318,000. Therefore, this corridor is a very busy and important highway network in this region and have major implications in the business around it.

1.2.Literature Review

The importance of reliable and safe lifeline systems for proper functioning of a society is well understood and realized by the research community. Therefore, there have been major research efforts, in the past decade and a half, to quantify the hazard and analyze the risk in different lifeline systems for understanding and efficiently mitigating the risk. Pacific Earthquake Engineering Research Centre (PEER) has been in the forefront to facilitate research in the area of lifeline seismic risk analysis and it has been put forward as one of its thrust areas. Transportation networks being one of the most important lifeline systems in a society, there have been efforts from the research community to effectively carry out seismic risk analysis in transportation network systems.

As a part of the research efforts of Pacific Earthquake Engineering Research Centre (PEER) on seismic performance assessment, Cornell and Krawlinker (2000) proposed the PEER framework equation for loss estimation which is discussed in the previous section. Many researchers have discussed and worked in this framework for a comprehensive way to quantify loss and boost performance based earthquake engineering. [e.g. Krawlinker and Miranda, (2004); Krawlinker (2004); Baker and Cornell (2003); Comerio (2004)]. Deierlein (2004) discusses this framework in detail and discusses the intermediate steps of the integral and the uncertainties associated with it. Miranda et al., (2004) proposes an approach to describe seismic performance of a building in terms of economic losses. Porter and Beck (2004) introduced a parameter to assess the seismic performance of a building called PFL (Probable Frequent Loss) which can be applied in financial analysis. Although these researches provide ways to quantify the loss in terms of dollars but most of it were valid only for a building.

There have been efforts to modify the methodologies required to carry out probabilistic seismic hazard analysis (PSHA). Gutenberg and Richter (1956) proposed the magnitude-frequency relationship which is widely used as a founding step to carry out PSHA and is popularly referred to as Gutenberg-Richter recurrence law. Due to the availability of better geologic data and understanding of the earth's crustal behavior, Schwartz and Coppersmith (1985) suggested the characteristic earthquake event procedure for magnitude-frequency relation. Wells and Coppersmith (1994) proposed the magnitude and area relationships which are widely used in PSHA calculations. The USGS WG 03 report on Earthquake Probabilities in the San Francisco Bay Region: 2002-2031 outlines the procedure to carry out PSHA and discusses every step in detail. Boore (2003) came up with the stochastic ground motion model which can be employed in PSHA. Dabaghi and Der Kiureghian (2014) have provided methods for stochastic modelling and simulation of near fault ground motions for PBEE. The usage of stochastic earthquake catalog in simulated PSHA has also been discussed.

Ground motion prediction equations (GMPE) are an important component of PSHA calculations. Major efforts have been put in place to come up with comprehensive set of equations to effectively model the ground motion intensities from source characterizations [e.g. Idriss (1991, 1994); Sadigh et al., (1997);

Abrahamson and Silva (1997); Campbell (1997, 2000, 2001); Atkinson and Boore (1997)]. The efforts of PEER in coming up with GMPE have resulted in the documentation of NGA (New Generation Attenuation) West and East database.

Seismic risk analysis methodologies for transportation systems have been presented by many researchers in the past [e.g. Kiremidjian et al., (2002); Chang et al., (2002); Werner et al., (1997)]. Werner et al., (2000) came up with new methodologies for deterministic and probabilistic ways of seismic risk analysis of highway networks with support from Federal Highway Administration for application in highway network nationwide. Eguchi et al., (2003) validated the seismic risk analysis methodology with case studies. Padgett and DesRoches (2007) provided a bridge functionality relationship for seismic risk analysis in a transportation network. Werner et al., (2003) developed the methodology they proposed into a public domain software named REDARS (**R**isk from **E**arthquake **DA**mage to **R**oadway **S**ystems). Moore et al., (2006) proposed a methodology to quantify the economic losses from travel forgone following a major earthquake. O'Connor et al., (2010) in the MCEER report laid out the guidelines for post-earthquake bridge inspection and gives insights into the time required for bridge inspection for different damage states following an earthquake.

1.3.Scope and Organization of the Thesis

As discussed in the previous section, this work aims at looking at the effect of low and moderate ground motion intensities in transportation networks. Travel time is most often considered to be the performance characteristic of a transportation network and it is highly dependent on the downtime of the network. Downtime in the transportation network due to any seismic event increases the travel time which is an implication of monetary loss. In the advancement of performance based earthquake engineering (PBEE) in the past decade, economic loss has been considered as one of the pivotal aspects and hence it is important to learn about economic loss for any seismic event to help decision makers to make well informed decisions.

Keeping this in view, this thesis proposes to come up with annual economic loss probabilities for low to moderate ground motion intensities.

The thesis has been divided into 5 chapters. Chapter 2 discusses the various methodologies used for conducting the PSHA and provides the data used and computed in this process. Chapter 3 explores the different aspects of traffic simulation. The traffic data used to carry out the traffic simulation has been presented and travel time delay data computed from the simulation has been presented. The correlation between travel time delay and economic loss is also discussed in this chapter. Chapter 4 integrates all the data from PSHA and traffic simulation to come up with a meaningful result in the form of a mean annual rate of exceedance curve. Chapter 5 draws conclusion from the data and results presented in the earlier chapters.

CHAPTER 2

SEISMIC HAZARD ANALYSIS FOR THE SR-91 CORRIDOR

2.1. Background

The risk assessment of any infrastructure system due to seismic events depends primarily on the ground motion that each event creates at any critical location of the infrastructure system and consequently on the effect of the ground motion on the infrastructure systems. Probabilistic Seismic Hazard Analysis (PSHA) as put forward by Cornell in 1968 gives a tool to reasonably quantify the uncertain level of ground shaking at a given location. The PSHA procedure takes into account all possible sources of seismic excitation and calculates the resulting ground motion intensity measure in a probabilistic framework. In a broad sense, the PSHA procedure includes characterization of the seismic sources, distribution of distance between the source and the site, prediction of the resulting ground motion intensity, and finally combining uncertainties in the seismic source, location and ground motion intensity. The techniques used in PSHA are discussed in a detailed way in the following sections.

2.2. Seismic Source Characterization

In conducting PSHA every seismic source surrounding the site of interest is taken into consideration. In this project, the highway network that we are considering is the California State Route 91 (SR-91). The bridges in the highway network are considered to be the most vulnerable sites in the system, and SR-91 has ten bridges. The list of the bridges along with the location and site property (V_{s30}) are presented in Table 2.1.

Table 2.1. Bridge Site Locations and Site Properties

Site No	Site Location	Latitude	Longitude	V_{s30}
1	Santa Ana Freeway	33.857121	-117.98041	230
2	Brookhurst Street	33.853934	-117.959213	280
3	Euclid Street	33.854119	-117.94175	280
4	East Street	33.853853	-117.906774	280
5	State College Boulevard	33.854232	-117.889361	280
6	Orange Freeway	33.849846	-117.875833	280
7	Costa Mesa Freeway	33.844146	-117.828324	354
8	Imperial Highway	33.854382	-117.790541	354
9	South Weir Canyon Road	33.87049	-117.744652	390
10	Jeep Trail	33.866873	-117.711484	354

For simplifying the required computational effort, the major seismic faults around SR-91 is considered as seismic sources. Massive efforts carried out by United States Geological Survey (USGS) over the years have resulted in very detailed information about active and quaternary faults located in the United States of America. The seismic faults are again divided into fault segments to indicate the shortest section considered to be ruptured repeatedly to generate major seismic events. For example, the San Andreas fault extends roughly 1300 km but the entire fault does not rupture at once, rather different segments of the fault ruptures at once or as a combination of these segments. Therefore, the USGS database has divided the San Andreas fault into nine fault segments. The location of the bridges and the seismic fault zones are represented in Figure 2.1.

Figure 2.1: Location of the Seismic Faults and Bridge Sites

The USGS database for seismic faults has detailed geological data regarding the slip rate, length, dip and characteristic magnitude of each seismic fault. Geological data of the seismic faults in California is also documented by California Geological Survey (CGS) in line with USGS database [Peterson et al., 1996]. With the transportation network being SR-91, five major faults surrounding the network has been considered for carrying out PSHA. These five faults are again divided into different segments as per the data available with USGS and CGS. The segments may rupture independently and as a combination of two or more segments at a time of a particular fault. The seven major seismic faults which fall in the 50 km radius from the sites of interest are considered for this work and are represented along with their properties in Table 2.1.

Table 2.2. Geological Data of Seismic Faults in consideration (Source: California Geological Society)

Fault No	Fault Name	Length (km)	Dip Down Width (km)	Slip Rate (mm/yr)	Characteristic Magnitude
1	Newport-Inglewood-Rose Canyon fault zone	64	13	1	6.9
2 (a)	Elsinore fault zone, Whittier section (Whittier fault)	37	15	2.5	6.8
2 (b)	Elsinore fault zone, Chino section (Chino fault)	28	17	1	6.7
2 (c)	Elsinore fault zone, Glen Ivy section	38	15	5	6.8
2 (d)	Elsinore fault zone, Temecula section	62	15	5	6.8
3	Hollywood fault	17	14	1	6.4
4	Raymond fault	21	13	0.5	6.5
5	Sierra Madre fault zone, Sierra Madre C section (Sierra Madre fault)	23	18	2	6.7
6	Palos Verdes fault zone, Santa Monica Basin section	96	13	3	7.1
7 (a)	San Andreas- San Bernardino	107	18	24	7.3
7 (b)	San Andreas- Southern	203	12	24	7.4
7 (c)	San Andreas-Mojave	99	12	30	7.1

These seven seismic faults give rise to 26 fault rupture scenarios because of the different combinations of fault segments rupturing together, which is also termed as cascading effect. The geologic

data viz. maximum magnitude and recurrence rate for all the rupture scenarios is necessary to carry out further steps of PSHA. The seismogenic area of all the rupture scenarios is estimated as

$$A = LWR \tag{2.1}$$

where L is the segment length, W is the down-dip segment width and R is the seismogenic scaling factor which ranges from 0 to 1. The seismogenic scaling factor R accounts for the aseismic rupture in the rupture source. The Hanks and Bakun (2001) model has been used to convert the segment and multi-segment areas to characteristic magnitude $\overline{M}_{char}$ for the rupture scenarios. This model is given as

$$\overline{M}_{char} = \begin{cases} 3.98 + \log_{10} A & for\ A \leq 468\ km^2 \\ 3.09 + \frac{4}{3}\log_{10} A & for\ A > 468\ km^2 \end{cases} \tag{2.2}$$

The moment balancing methodology explained in Appendix G of USGS WG 02 report has been employed in this work to estimate the slip rate of the rupture scenarios. The activity rate of the rupture scenarios is computed by balancing the long-term accumulation of moment with long term release. The seismic moment built up rate at any seismic fault is given by Aki (1997) and can be expressed as:

$$\frac{dM_0}{dt} = \mu A v \tag{2.3}$$

where, μ is the shear modulus, A is the seismogenic area as computed by Equation 2.1 and v is the slip rate of the fault segment in cm/year. Here, the shear modulus μ is considered to be $3\times10^{11}\ dyne/cm^2$ for all the seismic sources as suggested by USGS WG 02 report. The mean moment released in a characteristic earthquake is a function of the mean characteristic magnitude, $\overline{M}_{char}$ and the shape and truncation limits of the characteristic magnitude distribution. Here, the characteristic magnitude has been assumed to be having a Gaussian distribution truncated at $\pm\sigma_m$. The moment release in each characteristic earthquake event is given in USGS WG 02 report as

$$\overline{M}_{0char} = 10^{1.5\overline{M}_{char}+16.05-0.0481\sigma_m+1.775{\sigma_m}^2} \tag{2.4}$$

The total seismic moment released in a seismic fault can be expressed as the product of the moment release in each of the characteristic earthquake event and the rate of earthquake occurrences.

$$\overline{M}_{0char} \cdot v_m = \dot{M}_{released} \tag{2.5}$$

here, v_m is the rate of earthquake occurrences in the seismic fault. The moment release rate in the seismic fault can be equated with the moment built up rate of the same seismic fault.

$$\dot{M}_0 = \dot{M}_{released} = \mu A v \tag{2.6}$$

Therefore, the rate of earthquake occurrences can be expressed as,

$$v_m = \frac{\mu A v}{\overline{M}_{0char}} \tag{2.7}$$

The earthquake occurrence rate of each of the 26 seismic rupture scenarios are presented in the following table

Table 2.3. Rupture Sources and its corresponding characteristic magnitude and rate

Rupture Scenario	Rupture Source	$\overline{M}_{char}$	$\overline{M}_{0char}$	$\dot{M}_0$	Rate (/yr)
1	Newport-Inglewood-Rose Canyon fault zone	6.98	3.51E+26	2.5E+23	0.000712
2	Elsinore fault zone, Whittier section (Whittier fault)	6.74	1.56E+26	4.16E+23	0.002667
3	Elsinore fault zone, Chino section (Chino fault)	6.66	1.15E+26	1.43E+23	0.001244
4	Elsinore fault zone, Glen Ivy section	6.76	1.65E+26	8.55E+23	0.005193
5	Elsinore fault zone, Temecula section	7.04	4.38E+26	1.4E+24	0.003183
6	Elsinore fault zone, Whittier section (Whittier fault)+Elsinore fault zone, Chino section (Chino fault)	7.11	5.48E+26	5.46E+23	0.000996
7	Elsinore fault zone, Whittier section (Whittier fault)+Elsinore fault zone, Glen Ivy section	7.15	6.41E+26	1.27E+24	0.001973
8	Elsinore fault zone, Whittier section (Whittier	7.31	1.12E+27	1.67E+24	0.001495

	fault)+Elsinore fault zone, Temecula section				
9	Elsinore fault zone, Chino section (Chino fault)+Elsinore fault zone, Glen Ivy section	7.12	5.65E+26	9.5E+23	0.001682
10	Elsinore fault zone, Chino section (Chino fault)+Elsinore fault zone, Temecula section	7.30	1.05E+27	1.3E+24	0.001233
11	Elsinore fault zone, Glen Ivy section+Elsinore fault zone, Temecula section	7.32	1.14E+27	2.25E+24	0.001973
12	Elsinore fault zone, Whittier section (Whittier fault)+Elsinore fault zone, Chino section (Chino fault)+Elsinore fault zone, Glen Ivy section	7.34	1.21E+27	1.31E+24	0.001084
13	Elsinore fault zone, Whittier section (Whittier fault)+Elsinore fault zone, Chino section (Chino fault)+Elsinore fault zone, Temecula section	7.46	1.84E+27	1.62E+24	0.000879
14	Elsinore fault zone, Whittier section (Whittier fault)+Elsinore fault zone, Glen Ivy section+Elsinore fault zone, Temecula section	7.50	2.14E+27	2.57E+24	0.001201
15	Elsinore fault zone, Chino section (Chino fault)+Elsinore fault zone, Glen Ivy section+Elsinore fault zone, Temecula section	7.46	1.87E+27	2.11E+24	0.001132
16	Hollywood fault	6.35	4.02E+25	7.14E+22	0.001774
17	Raymond fault	6.41	4.94E+25	4.1E+22	0.000828
18	Sierra Madre fault zone, Sierra Madre C section (Sierra Madre fault)	6.49	6.39E+25	1.94E+23	0.003042
19	Palos Verdes fault zone, Santa Monica Basin section	7.21	7.89E+26	1.12E+24	0.001423
20	San Andreas- San Bernardino	7.46	1.88E+27	1.39E+25	0.007377
21	San Andreas- Southern	7.60	3.01E+27	1.75E+25	0.005833
22	San Andreas-Mojave	7.18	7.15E+26	1.07E+25	0.01495

23	San Andreas- San Bernardino +San Andreas- Southern	7.97	1.1E+28	3.35E+25	0.003056
24	San Andreas- San Bernardino +San Andreas-Mojave	7.74	4.84E+27	2.5E+25	0.005173
25	San Andreas- Southern+San Andreas-Mojave	7.83	6.66E+27	2.94E+25	0.004411
26	San Andreas- San Bernardino +San Andreas- Southern+San Andreas-Mojave	8.10	1.66E+28	4.47E+25	0.002688

2.3. Characteristic Earthquake Model

For probabilistic seismic hazard analysis quantifying the relation between earthquake magnitude and frequency is important. Traditionally the truncated exponential model proposed by Gutenberg and Richter in 1956 is adopted to quantify the recurrence of seismic events. This model is popularly known as Gutenberg-Richter magnitude recurrence relation and is expressed as:

$$\log \lambda_m = a - bm \tag{2.8}$$

here the value of a represents the rate of earthquake occurrence with magnitudes greater than zero. The b value is related to the relative likelihood of earthquakes with different magnitudes and typically takes a value between 0.8-1.0. Both these values are estimated using historical data and creating a catalog of historical earthquake occurrences. Although the Gutenberg-Richter recurrence law holds good for big seismic zones based on historical data, it is not as good in a fault source with available geologic data [Youngs and Coppersmith, 1985]. Because of this shortcoming, Schwartz and Coppersmith came up with another model referred to as the characteristic earthquake model in 1985. The basic assumption of this model is that a seismic fault would tend to generate the same size of earthquake or the "characteristic" earthquake magnitude. This assumption is based on the fact that a seismic fault of the same dimension with same geologic data would always tend to generate earthquake of a preferred magnitude which is referred to as characteristic earthquake. Empirical data has shown that 94% of the seismic energy is released through the characteristic earthquake [Abrahamson, 2006]. Although this characteristic earthquake has a variability due to aleatory uncertainty. Therefore, a truncated normal distribution of magnitudes with the characteristic

magnitude as the mean and truncated at a standard deviation is used to accommodate the aleatory uncertainty in the model. This model of Characteristic Earthquake Model is adopted here to carry out the seismic hazard analysis. The truncated normal distribution for characteristic earthquake model can be expressed as:

$$f_m^{TN}(M) = \begin{cases} \frac{1}{\sqrt{2\pi}\sigma_m} \cdot \frac{1}{\Phi(\sigma_{TN})} \cdot exp\left(\frac{-\left(M - \overline{M}_{char}\right)^2}{2\sigma_m^2}\right) & for \ \frac{-\left(M - \overline{M}_{char}\right)}{\sigma_m} < \sigma_{TN} \\ 0 & otherwise \end{cases} \quad (2.9)$$

here, σ_{TN} is the point at which the normal distribution is truncated and $\overline{M}_{char}$ is the characteristic earthquake for the seismic fault. As per recommendations of USGS WG 03, we assume that the distribution of the characteristic event of each rupture scenarios has a normal distribution with variance of ${\sigma_m}^2$ and it is truncated at $\pm\sigma_m$. The standard deviation of the distribution σ_m is considered to be 0.12 as suggested by the USGS WG 03 report. The mean characteristic magnitude of the distribution of each of the rupture scenarios has been given in Table 2.2. The probability density function of two of the rupture scenarios are shown in Figure 2.2 & Figure 2.3

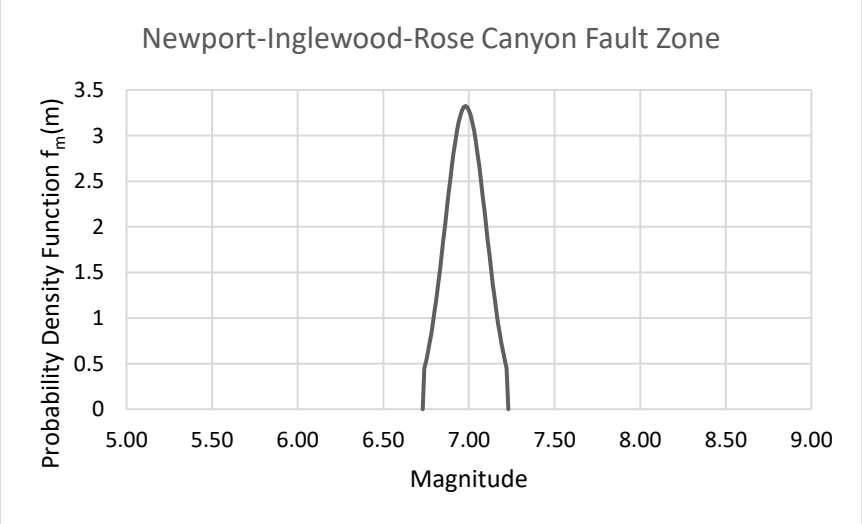

Figure 2.2. Distribution Characteristic Event for Rupture Scenario 1

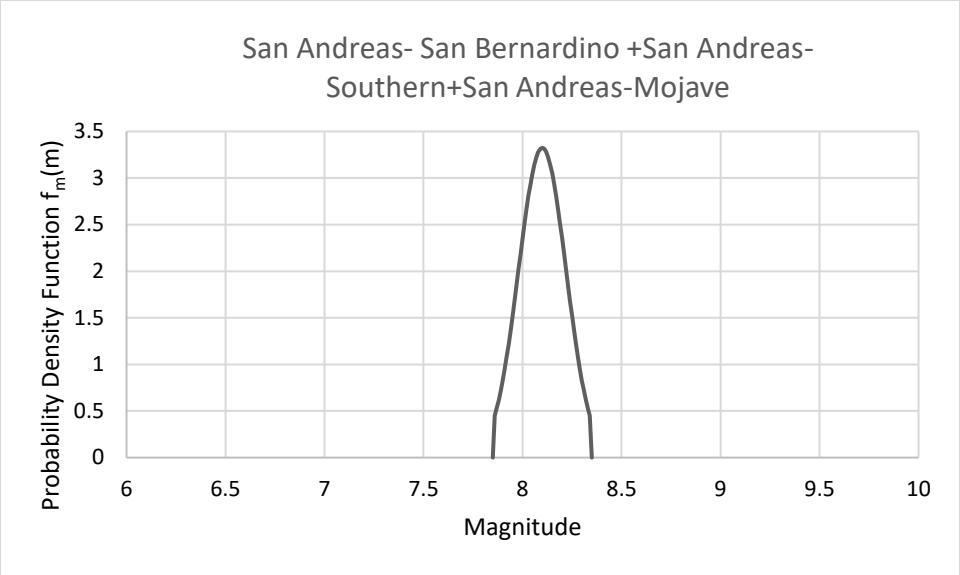

Figure 1.3. Distribution Characteristic Event for Rupture Scenario 26

2.3. Stochastic Earthquake Catalog

A stochastic earthquake catalog is built using the available data to carry out the probabilistic seismic hazard analysis. Monte Carlo simulation procedure is used to build this earthquake catalog as used by Crowley and Boomer [2006] and by Yamamoto and Baker [2011]. The stochastic earthquake catalog is a list of all possible realization of earthquake events that may take place in the future Y years. The application of Monte Carlo simulation brings in the inherent assumption that the rupture scenarios are homogeneous Poisson events and that the seismic characterization of the rupture source doesn't change over the period of time. A realization of earthquake events in a 10,000-year period has been prepared with the assumptions cited above. For each of the rupture scenarios the mean annual rupture rate has already been calculated in the section above. Therefore, the probability of rupture in one year is drawn from a Poisson distribution with mean $\lambda_i Y$, where λ_i is the mean annual rupture rate and Y is the no of year. Occurrence of the earthquake event is independent from year to year. The Poisson distribution can be expressed as,

$$p_x(x) = (\lambda_i Y)^x \cdot \exp(-\lambda_i Y)/x! \tag{2.9}$$

where, x is the event of earthquake event occurrence in a single year. The probability of occurrence of one earthquake event in one year is calculated ($i.e. x = 1; Y = 1$) from Equation 2.9. With the probability of earthquake occurrence computed for all the rupture scenarios, the no of possible ruptures for each of the scenarios for a period of 10,000 years are randomly picked using Monte Carlo simulation. This procedure gave a catalog of 732 earthquake events across all the 26 rupture scenarios for a period of 10,000. The following table represents the possible no of ruptures for each of the 26 rupture scenarios:

Table 2.4. Rupture Sources and total no of ruptures in the catalog

Rupture Scenario	**Rupture Source**	$\overline{M}_{char}$	**Rate (/yr)**	**Total No of Ruptures N_i**
1	Newport-Inglewood-Rose Canyon fault zone	6.98	0.000712	9
2	Elsinore fault zone, Whittier section (Whittier fault)	6.75	0.002667	24
3	Elsinore fault zone, Chino section (Chino fault)	6.66	0.001244	9
4	Elsinore fault zone, Glen Ivy section	6.76	0.005193	57
5	Elsinore fault zone, Temecula section	7.05	0.003183	24
6	Elsinore fault zone, Whittier section (Whittier fault) +Elsinore fault zone, Chino section (Chino fault)	7.11	0.000996	9
7	Elsinore fault zone, Whittier section (Whittier fault) +Elsinore fault zone, Glen Ivy section	7.16	0.001973	23
8	Elsinore fault zone, Whittier section (Whittier fault) +Elsinore fault zone, Temecula section	7.32	0.001495	16
9	Elsinore fault zone, Chino section (Chino fault) +Elsinore fault zone, Glen Ivy section	7.12	0.001682	19
10	Elsinore fault zone, Chino section (Chino fault) +Elsinore fault zone, Temecula section	7.30	0.001233	10
11	Elsinore fault zone, Glen Ivy section+Elsinore fault zone, Temecula section	7.32	0.001973	18
12	Elsinore fault zone, Whittier section (Whittier fault) +Elsinore fault zone, Chino section (Chino fault) +Elsinore fault zone, Glen Ivy section	7.34	0.001084	13

13	Elsinore fault zone, Whittier section (Whittier fault) +Elsinore fault zone, Chino section (Chino fault) +Elsinore fault zone, Temecula section	7.46	0.000879	13
14	Elsinore fault zone, Whittier section (Whittier fault) +Elsinore fault zone, Glen Ivy section+Elsinore fault zone, Temecula section	7.51	0.001201	8
15	Elsinore fault zone, Chino section (Chino fault) +Elsinore fault zone, Glen Ivy section+Elsinore fault zone, Temecula section	7.47	0.001132	11
16	Hollywood fault	6.36	0.001774	21
17	Raymond fault	6.42	0.000828	2
18	Sierra Madre fault zone, Sierra Madre C section (Sierra Madre fault)	6.49	0.003042	25
19	Palos Verdes fault zone, Santa Monica Basin section	7.22	0.001423	11
20	San Andreas- San Bernardino	7.47	0.007377	61
21	San Andreas- Southern	7.61	0.005833	60
22	San Andreas-Mojave	7.19	0.01495	136
23	San Andreas- San Bernardino +San Andreas-Southern	7.98	0.003056	41
24	San Andreas- San Bernardino +San Andreas-Mojave	7.74	0.005173	39
25	San Andreas- Southern+San Andreas-Mojave	7.84	0.004411	45
26	San Andreas- San Bernardino +San Andreas-Southern+San Andreas-Mojave	8.10	0.002688	28

Each event for all the rupture scenario is uniquely defined with a magnitude and a location. The magnitude is selected from the respective truncated Gaussian distribution of the characteristic earthquake event. And, the location of the earthquake is assumed to be uniformly distributed along the length of the fault in each of the rupture scenarios. The magnitude and the location are thus randomly picked and a stochastic catalog of 732 unique earthquake events are compiled for the seismic hazard analysis of the transportation network of interest.

The distribution of rupture distance and the magnitude computed as per the procedure discussed above for each of the ten bridge sites is shown in Figure 2.4-Figure 2.13

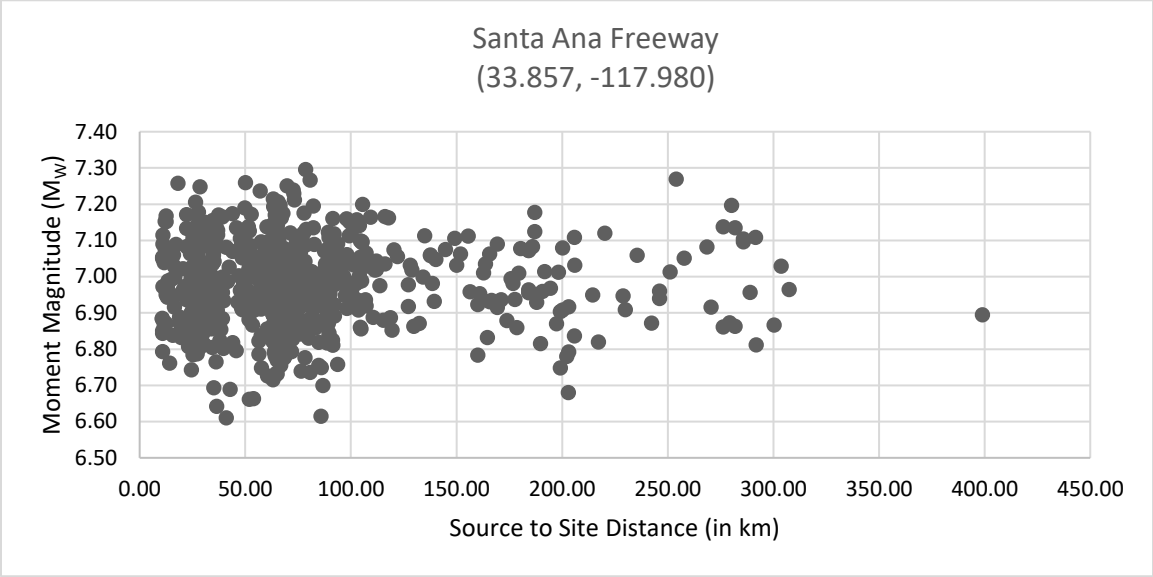

Figure 2.4. Distribution of Magnitude against Distance for Bridge Site 1

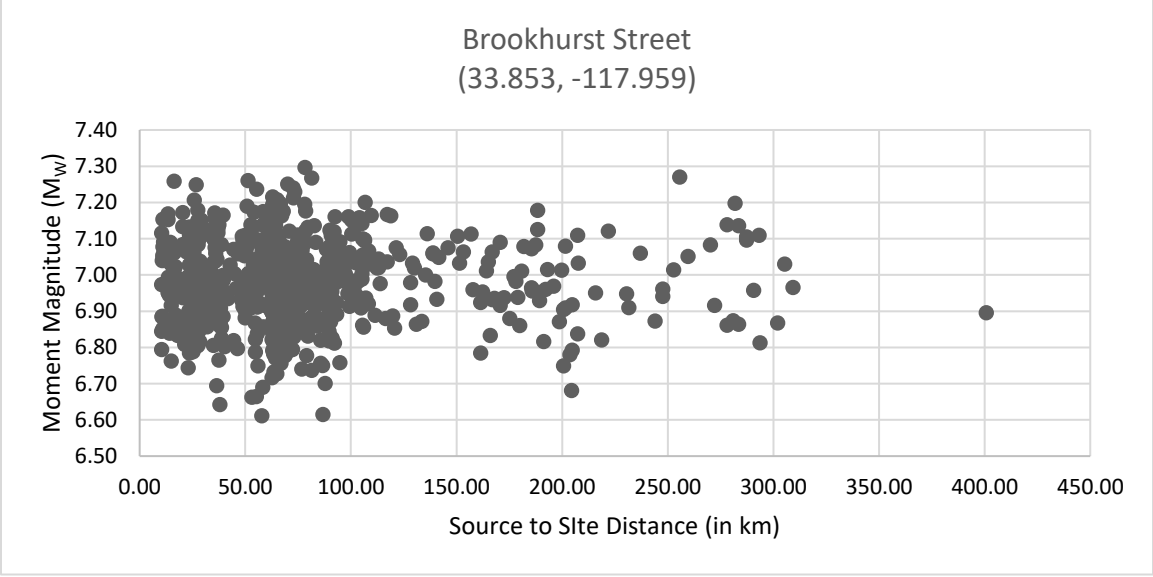

Figure 2.5. Distribution of Magnitude against Distance for Bridge Site 2

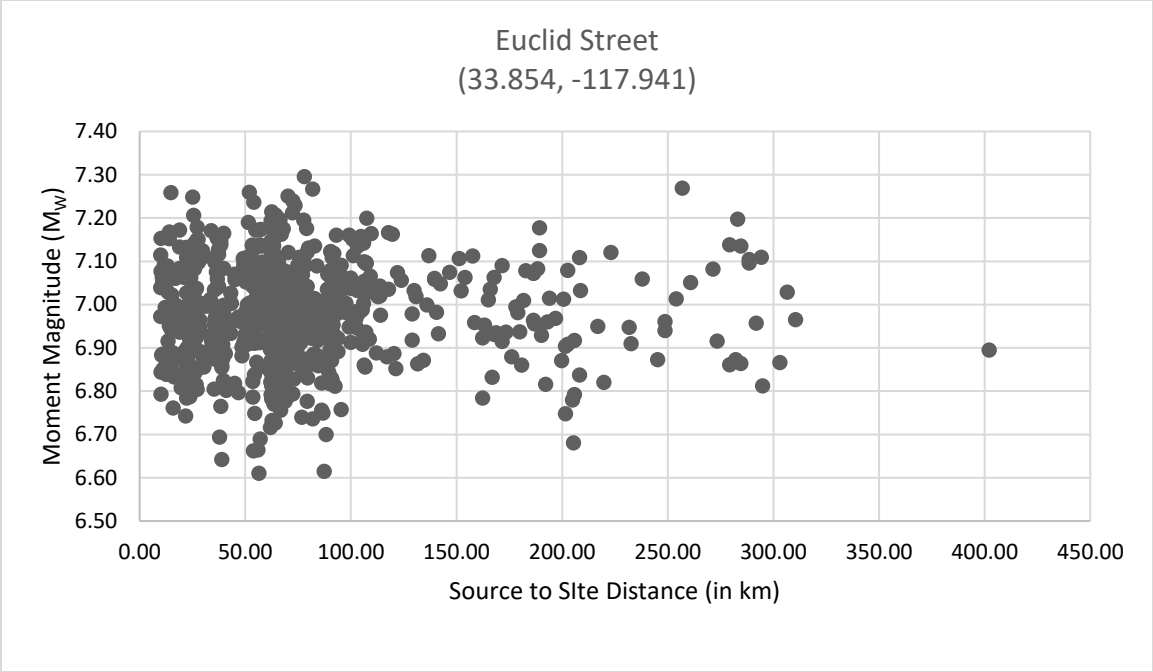

Figure 2.6. Distribution of Magnitude against Distance for Bridge Site 3

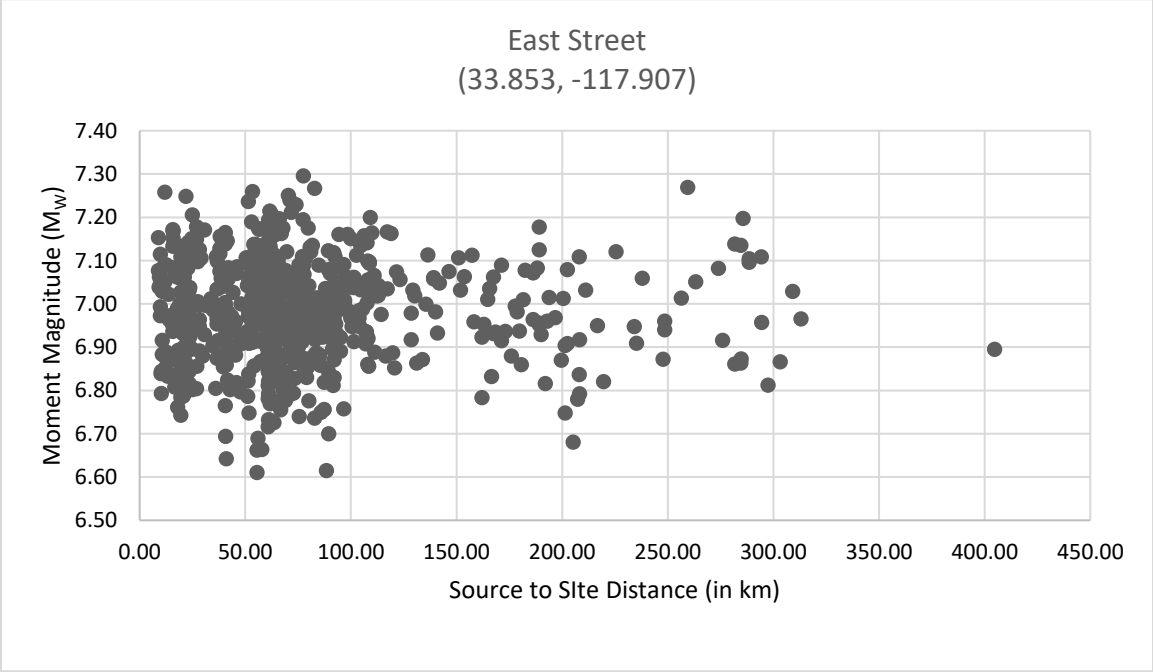

Figure 2.7. Distribution of Magnitude against Distance for Bridge Site 4

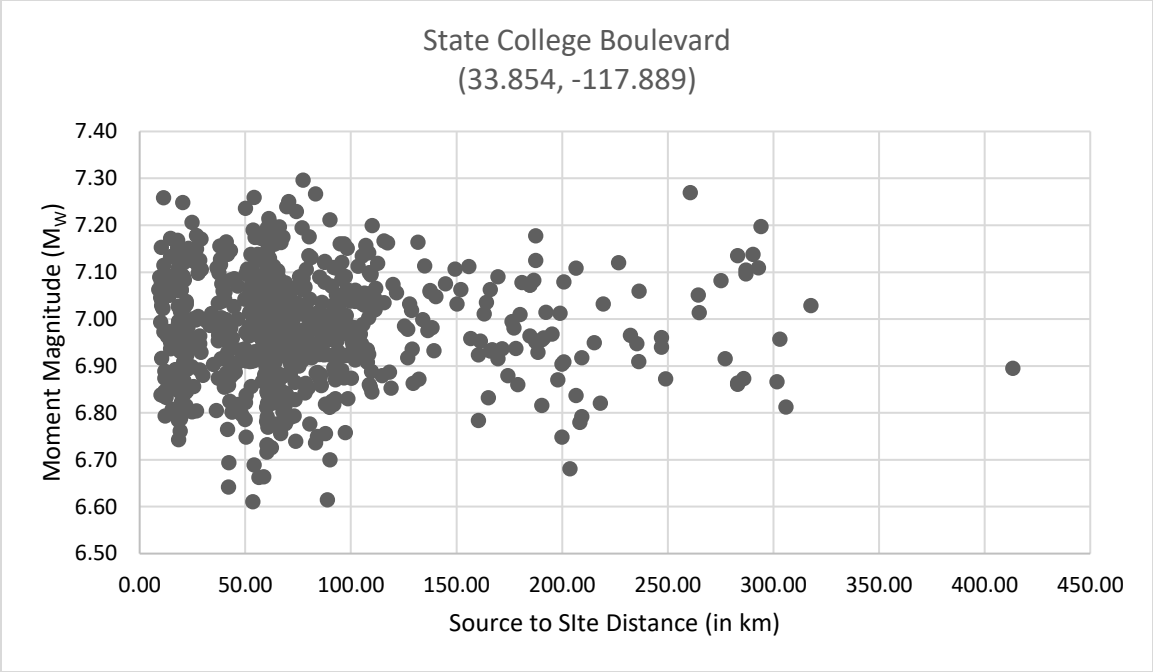

Figure 2.8. Distribution of Magnitude against Distance for Bridge Site 5

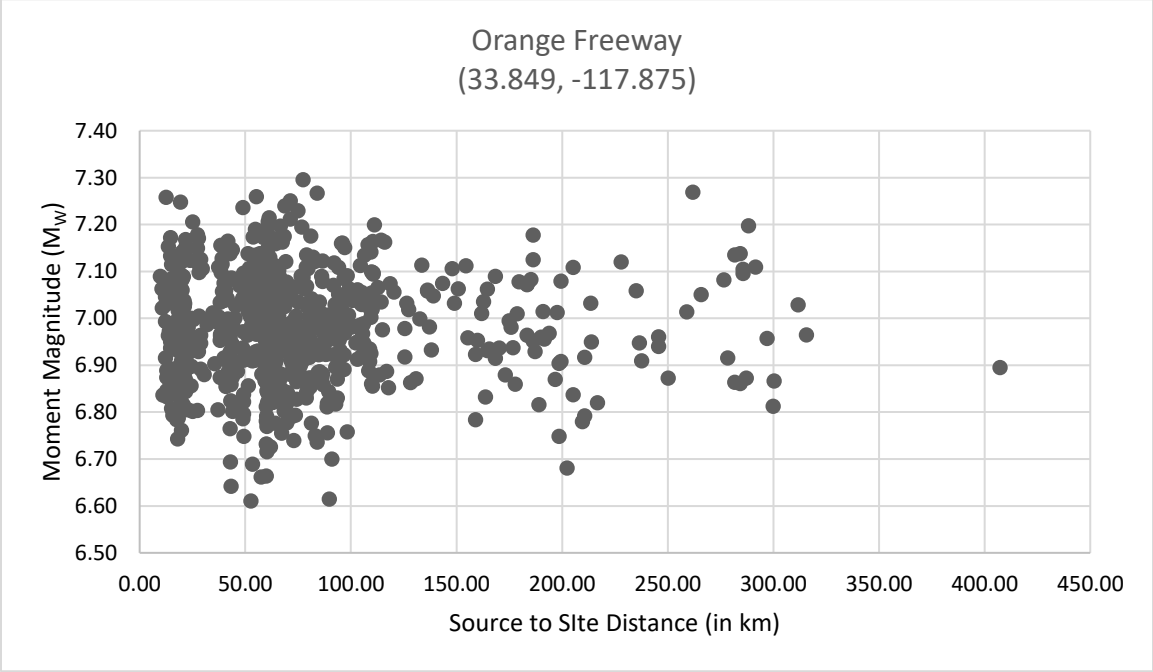

Figure 2.9. Distribution of Magnitude against Distance for Bridge Site 6

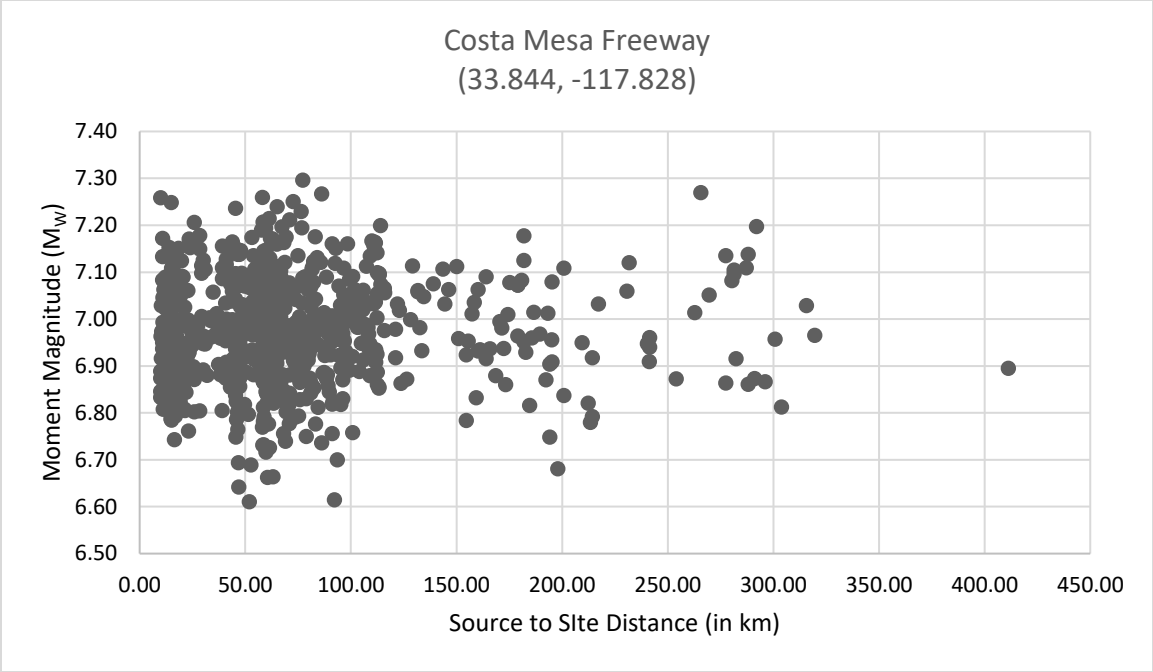

Figure 2.10. Distribution of Magnitude against Distance for Bridge Site 7

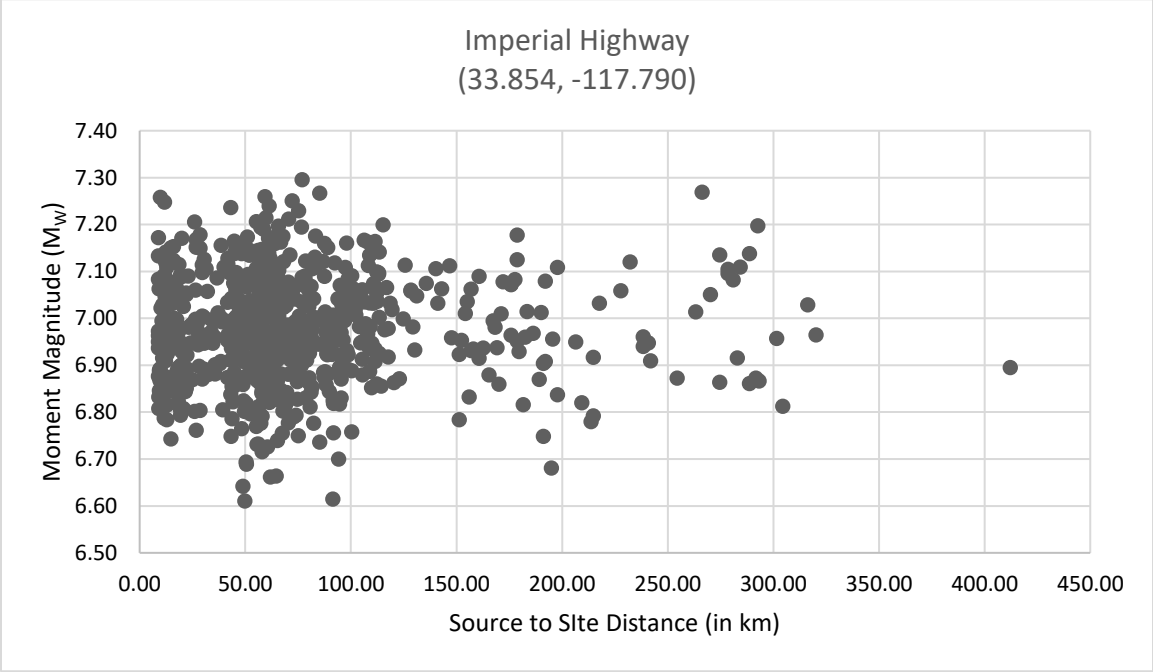

Figure 2.11. Distribution of Magnitude against Distance for Bridge Site 8

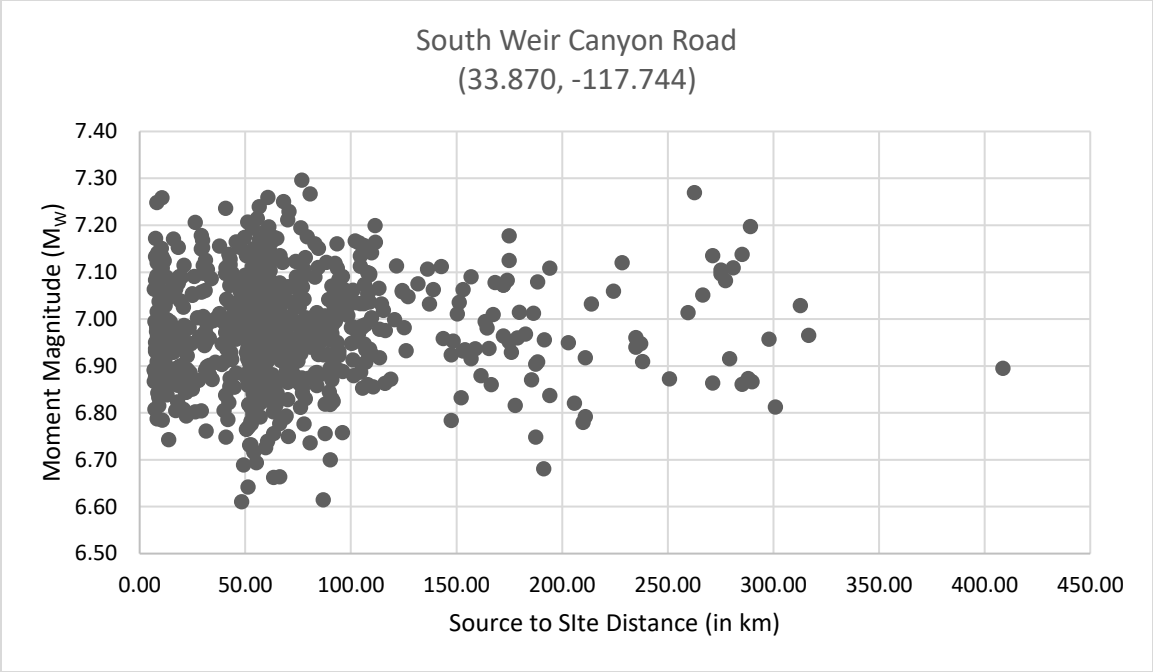

Figure 2.12. Distribution of Magnitude against Distance for Bridge Site 9

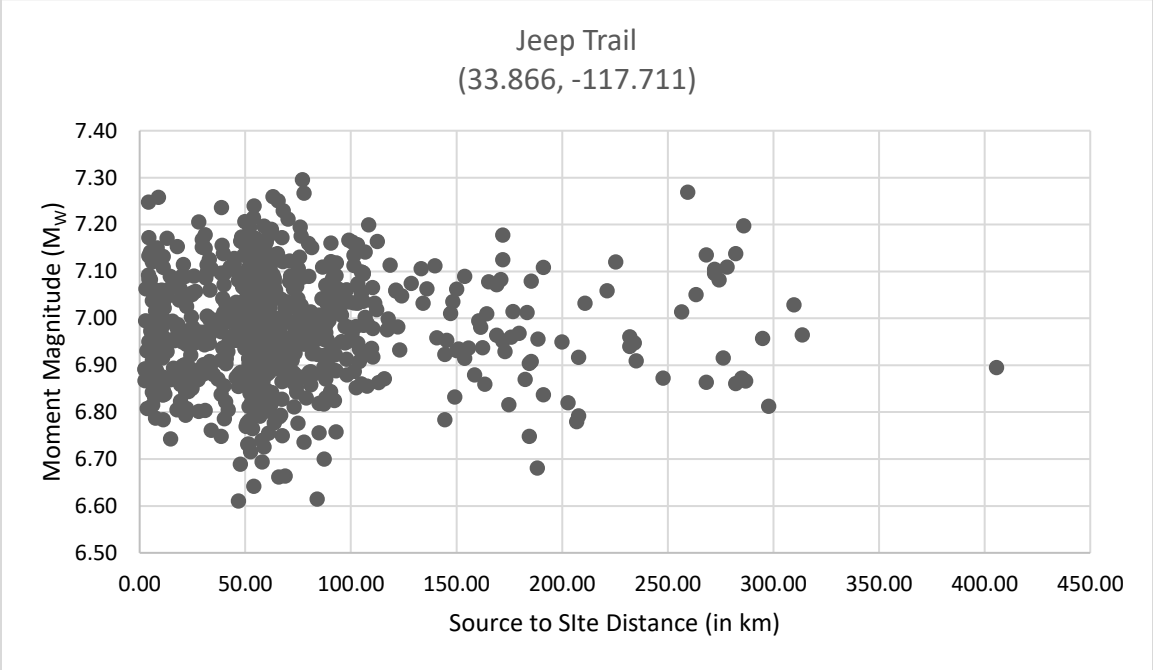

Figure 2.13. Distribution of Magnitude against Distance for Bridge Site 10

2.4. Ground Motion Model

Estimation of ground motion parameters at sites of interest is one of the most critical step of PSHA. There have been major efforts to correlate ground motion parameters to earthquake magnitude, location of the earthquake event and site specific properties. Ground motion parameters are critical to assess the performance of structures and quantify the hazard at sites of interest. The relationships developed to provide estimates of ground motion parameters from seismic source characteristics are broadly referred to as attenuation relationship.

Campbell and Bozorginia [2014] developed an empirical ground motion model based on the NGA-2 database. This model has been used in this work to predict the ground motion intensity measures at the bridge sites for all the 732 earthquake events in the stochastic earthquake catalog as discussed in Section 2.3. The Campbell and Bozorgnia [2014] attenuation relationship is of the following form:

$$\widehat{\ln Y} = f_{mag} + f_{dis} + f_{flt} + f_{hng} + f_{site} + f_{sed} \tag{2.10}$$

Where

f_{mag} is dependent on the magnitude and is given by,

$$f_{mag} = \begin{cases} c_o + c_1\mathbf{M}; & \mathbf{M} \leq 5.5 \\ c_o + c_1\mathbf{M} + c_2(\mathbf{M} - 5.5); & 5.5 < \mathbf{M} \leq 6.5 \\ c_o + c_1\mathbf{M} + c_2(\mathbf{M} - 5.5) + c_2(\mathbf{M} - 6.5); & \mathbf{M} > 6.5 \end{cases} \tag{2.11}$$

f_{dis} is dependent on the source to site distance and is given by,

$$f_{dis} = (c_4 + c_5\mathbf{M}) \ln\left(\sqrt{R_{RUP}^2 + {c_4}^2}\right) \tag{2.12}$$

f_{flt} is dependent on the source to site distance and is given by,

$$f_{flt} = \mathrm{c}_7 F_{RV} f_{flt,z} + c_8 F_{NM} \tag{2.12}$$

$$f_{flt,z} = \begin{cases} Z_{TOR}; & Z_{TOR} < 1 \\ 1; & Z_{TOR} > 1 \end{cases} \tag{2.13}$$

f_{hng} is dependent on the source to site distance and is given by,

$$f_{hng} = f_{hng,R} f_{hng,M} f_{hng,Z} f_{hng,\delta} \tag{2.14}$$

$$f_{hng,R} = \begin{cases} 1; & R_{JB} = 0 \\ \left[\max\left(RR_{RUP}, \sqrt{R_{JB}^2 + 1}\right) - R_{JB}\right] \Big/ max\left(R_{RUP}, \sqrt{R_{JB}^2 + 1}\right); & R_{JB} > 0, Z_{TOR} < 1, \\ \left(R_{RUP} - R_{JB}\right)/R_{RUP}\,; & R_{JB} > 0, Z_{TOR} \geq 1 \end{cases} \tag{2.15}$$

$$f_{hng,M} = \begin{cases} 0; & \mathbf{M} \leq 6.0 \\ 2(\mathbf{M} - 6.0); & 6.0 < \mathbf{M} < 6.5, \\ 1; & \mathbf{M} \geq 6.5 \end{cases} \tag{2.16}$$

$$f_{hng,Z} = \begin{cases} 0; & Z_{TOR} \geq 20 \\ (20 - Z_{TOR})/20; & 0 \leq Z_{TOR} \leq 20 \end{cases} \tag{2.17}$$

$$f_{hng,\delta} = \begin{cases} 1; & \delta \leq 70 \\ (90 - \delta)/20; & \delta > 70 \end{cases} \tag{2.18}$$

f_{site} is dependent on shallow linear and nonlinear site conditions and is given by,

$$f_{site} = \begin{cases} c_{10} \ln\left(\frac{V_{S30}}{k_1}\right) + k_2 \left\{\ln\left[A_{1100} + c\left(\frac{V_{S30}}{k_1}\right)^n\right] - \ln[A_{1100} + c]\right\}; & V_{S30} < k_1 \\ (c_{10} + k_2 n) \ln\left(\frac{V_{S30}}{k_1}\right); & V_{S30} \geq k_1 \end{cases} \tag{2.19}$$

f_{sed} is dependent on shallow sediment effects and 3-D basin effects and is given by

$$f_{sed} = \begin{cases} c_{11}(Z_{2.5} - 1); & Z_{2.5} < 1 \\ 0; & 1 \leq Z_{2.5} \leq 3 \\ c_{12} k_3 e^{-0.75}\left[1 - e^{-0.25(Z_{2.5} - 3)}\right]; & Z_{2.5} \leq 3 \end{cases} \tag{2.20}$$

$\widehat{\ln Y}$ represents the natural logarithm of the median value of the intensity measure of interest which can be horizontal peak ground acceleration (PGA) in g, peak horizontal ground velocity (PGV) in cm/sec, peak horizontal ground displacement (PGD) in cm or horizontal 5%-damped pseudo absolute acceleration (SA) in g in terms of the new geometric mean measure GMRotI50. [Campbell and Bozorgnia, 2014].

In this work, natural logarithmic of the median value of the peak ground acceleration(PGA) has been adopted as the ground motion intensity measure. A MATLAB code has been written to implement the attenuation relationship and it has been used to estimate the ground motion intensity for each of the ten

bridge sites in the network in all the 732 earthquake events. For simplifying the computation effort, all the fault segments are considered to be a strike slip fault. The distribution of PGA with respect to the moment magnitude at each of the site for all the earthquake events are presented in Figure 2.14-Figure 2.23:

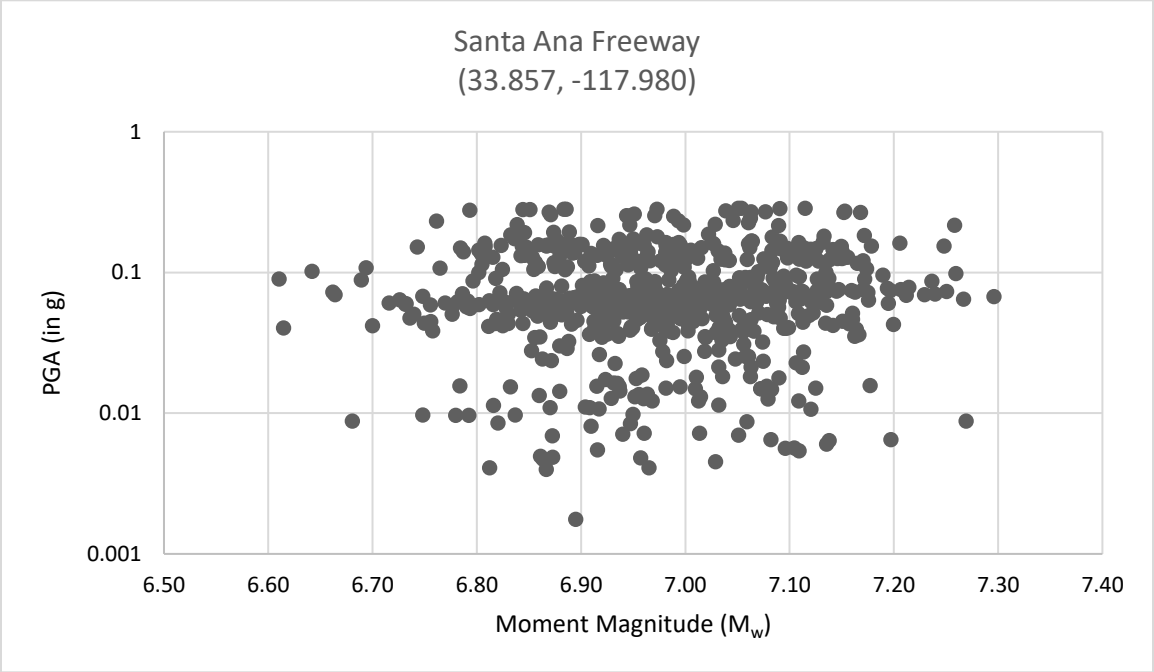

Figure 2.14. Distribution of PGA against Magnitude for Bridge Site 1

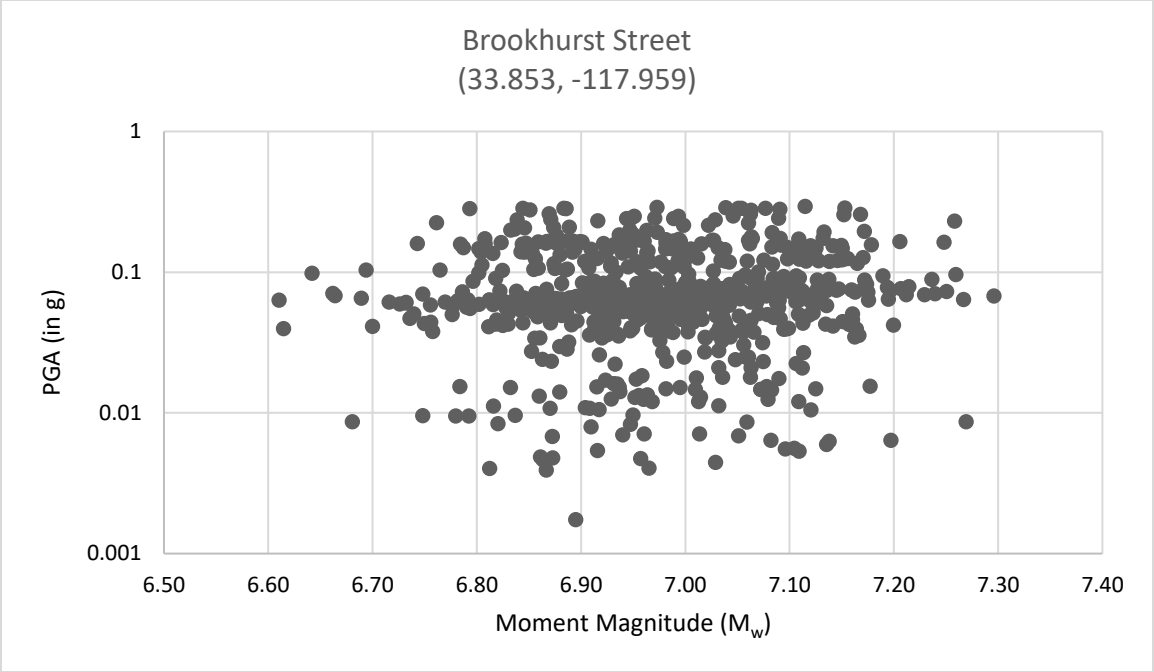

Figure 2.15. Distribution of PGA against Magnitude for Bridge Site 2

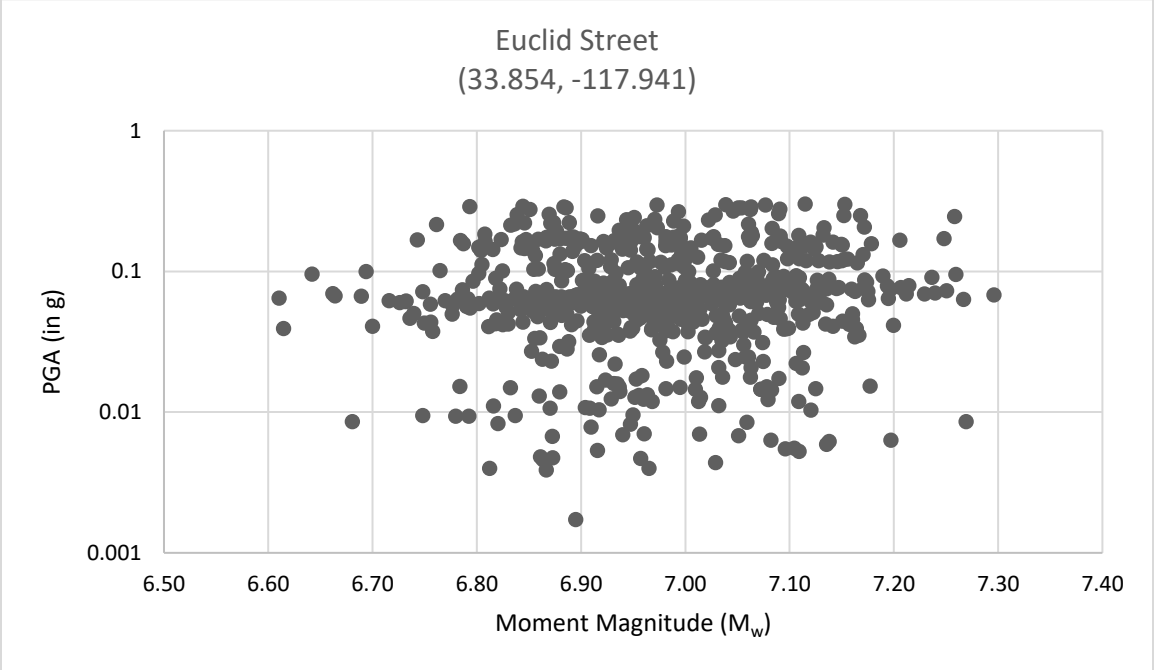

Figure 2.16. Distribution of PGA against Magnitude for Bridge Site 3

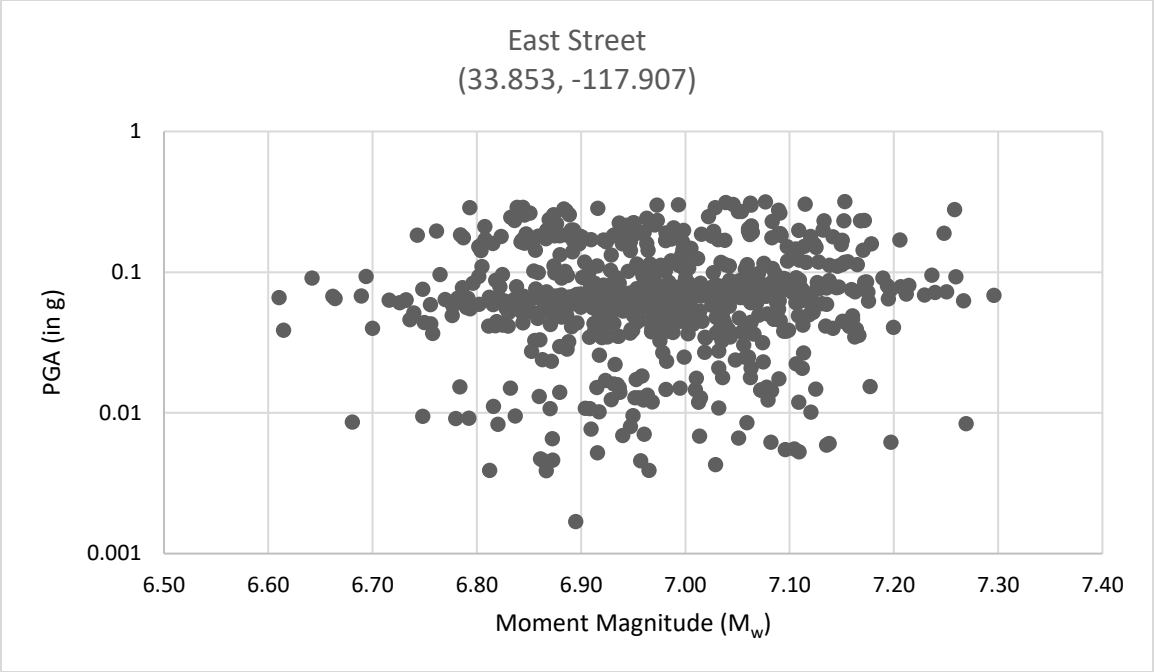

Figure 2.17. Distribution of PGA against Magnitude for Bridge Site 4

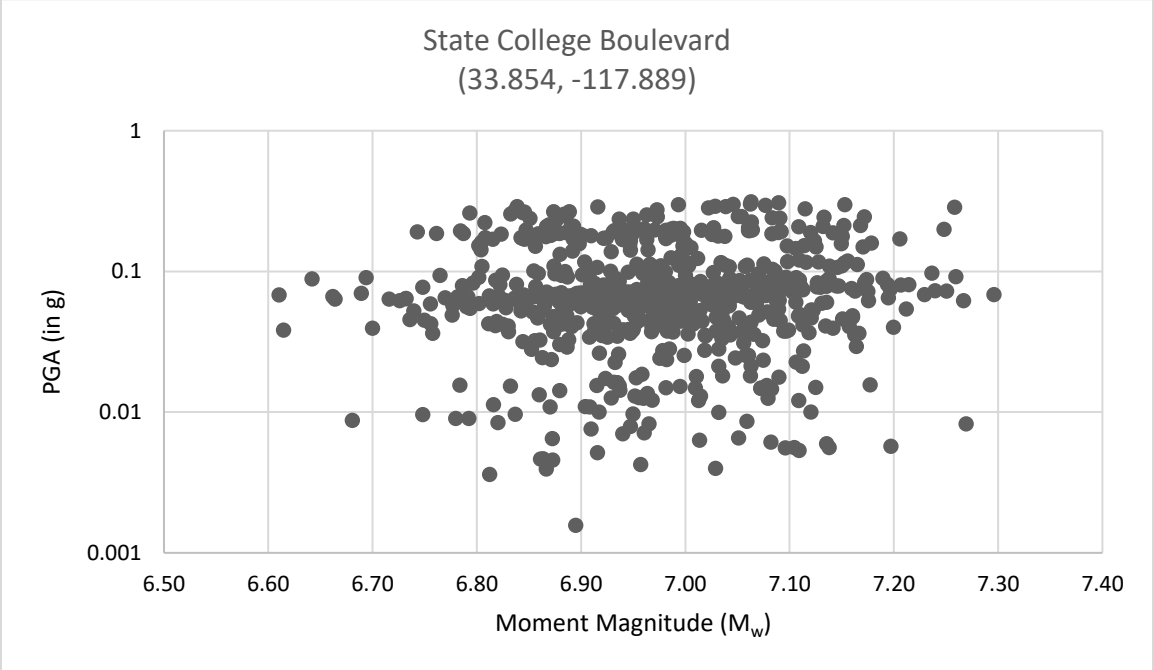

Figure 2.18. Distribution of PGA against Magnitude for Bridge Site 5

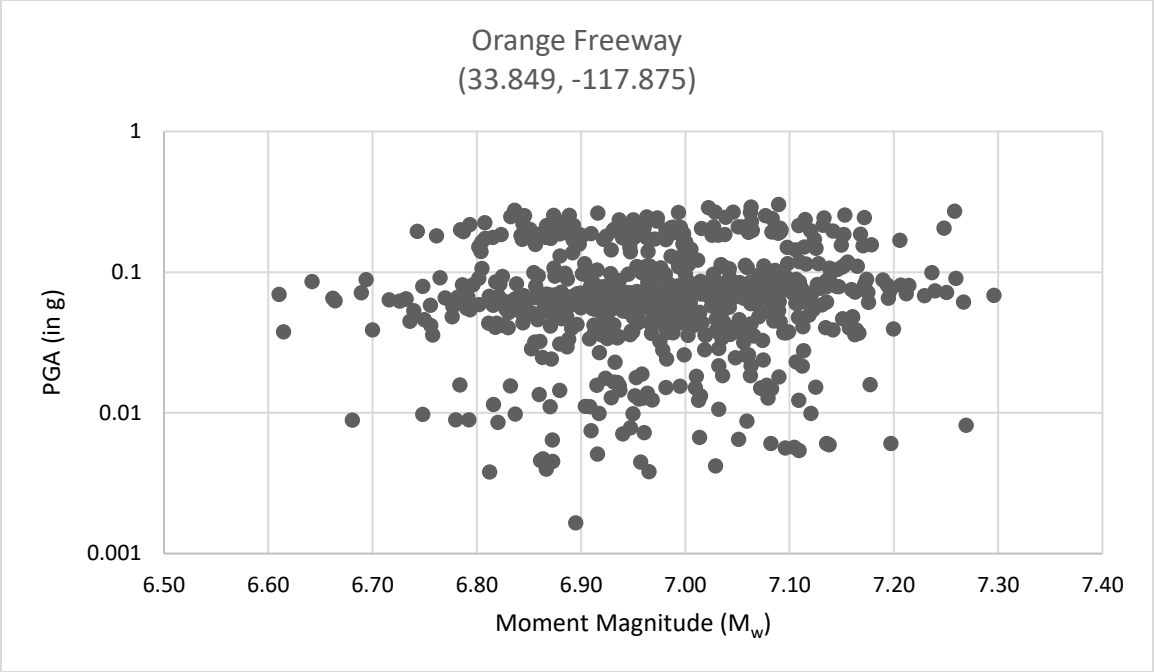

Figure 2.19. Distribution of PGA against Magnitude for Bridge Site 6

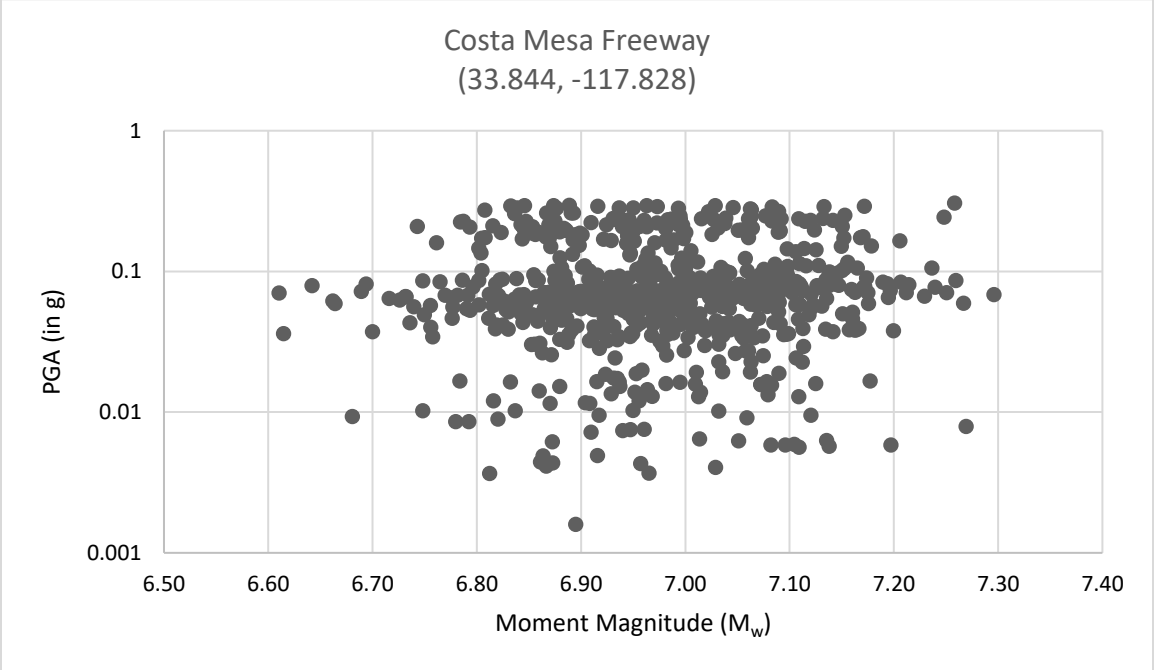

Figure 2.20. Distribution of PGA against Magnitude for Bridge Site 7

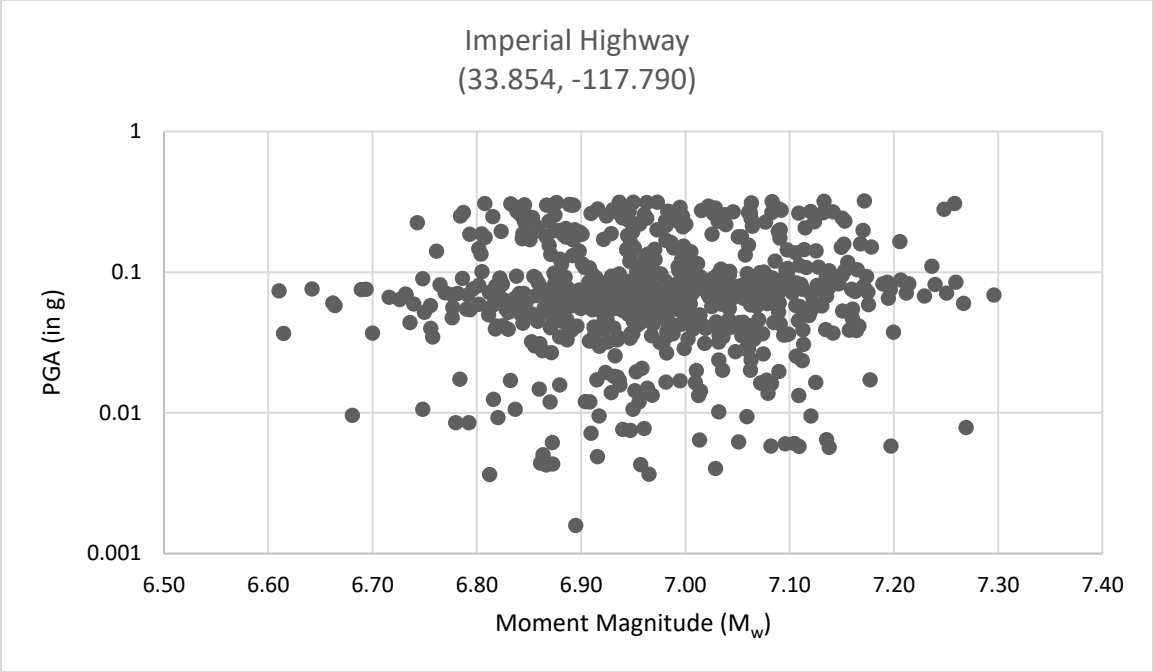

Figure 2.21. Distribution of PGA against Magnitude for Bridge Site 8

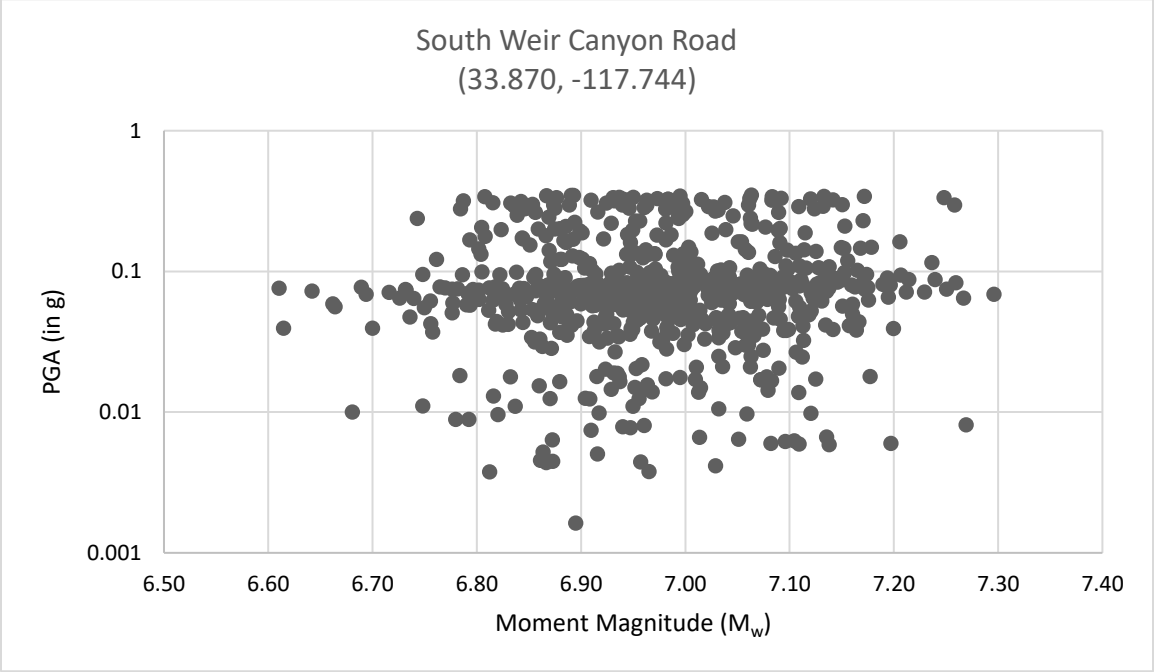

Figure 2.22. Distribution of PGA against Magnitude for Bridge Site 9

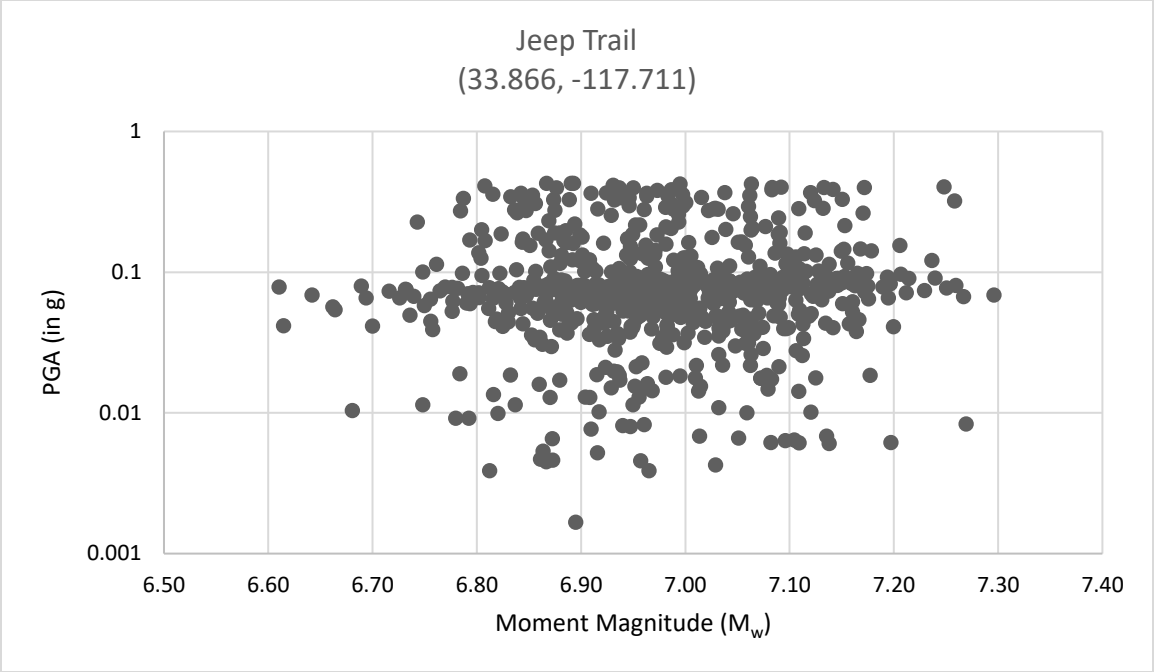

Figure 2.23. Distribution of PGA against Magnitude for Bridge Site 10

2.5. Bridge Fragility and Relation Between IM and Damage State

Bridge fragility relationships are established to estimate the performance of the bridges given the ground motion intensities computed at the bridge sites. There have been major efforts in the earthquake engineering research community to come up with comprehensive fragility relationships for different bridge types [e.g. Hwang et al., 2000; Gardoni et al., 2002; Shinozuka et al., 2003; Choi et al., 2004; Mackie and Stojadinovic 2004; Nielson and DesRoches 2007, Padgett and DesRoches 2008, Zakeri et al., 2014 etc]. The bridges on the SR-91 corridor are considered to fall in the category of Multi-Span Continuous Concrete Box-Girder (MSCC-BG) bridges. The generality of MSCC-BG type of bridges in California and the availability of fragility relation for this type of data is the basis of this assumption. The fragility curve data used in this work has been developed by Zakeri and Zareian, (2017) in their work related to bridge design framework for target seismic loss. Two damage states are defined for the purpose of this work as slight damage and moderate damage. Damages in three performance groups are considered while defining the damage states, i.e. shear keys, approach slabs and deck rotation. The limit states for the components are

defined as per the research conducted by Mackie et al., (2008). Slight damage in the bridge is defined when the most severe damage in one or more component is slight damage which corresponds to DS0 defined by Mackie, (2008) and moderate damage is when the most severe damage in the components of the bridge corresponds to DS1. It is also taken care of that no other component causes structural damage to the bridge while defining these damage states. The cumulative density function (CDF) of engineering demand parameter (EDP) and ground motion intensity (IM) and the cumulative density function (CDF) of damage state (DS) and engineering demand parameter (EDP) for MSCC-BG has been established in Zakeri and Zareian, (2017). From these relationships, the CDF of the damage states defined above given the IM has been established and is presented in Figure 2.24:

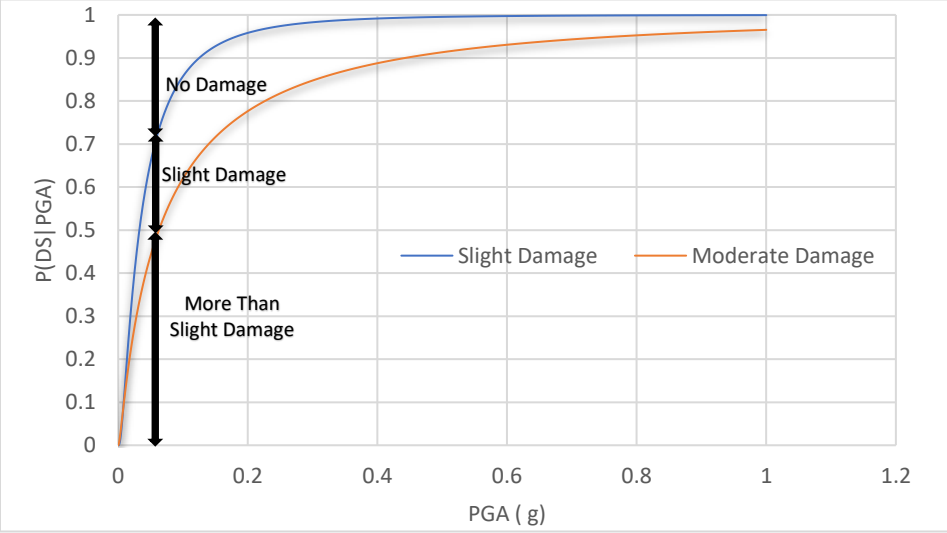

Figure 2.24. Cumulative Distribution Function of probability of being in Damage State (i.e. Slight Damage or Moderate Damage) given the PGA at the site

The damage in a highway network corresponds to the worst damage state of the bridges. This work emphasizes on the highway network being in slight damage state. Therefore, the scope of this work is limited to the scenarios when the most severe damage of a bridge in the network falls in the slight damage state. If any bridge in the network has suffered more than slight damage, the scenario is out of the scope of this work and the losses are assumed to be infinite. An illustration of the damage in a highway network is given in Figure 2.25

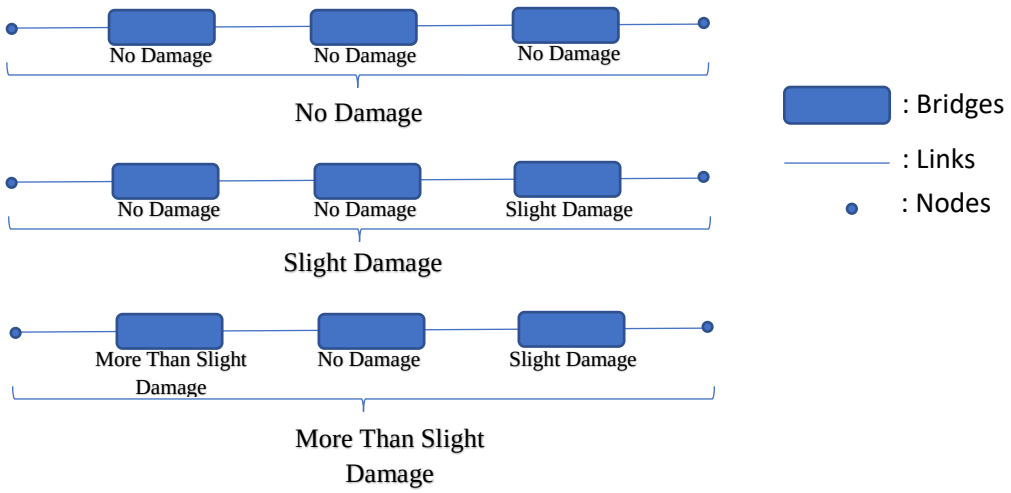

Figure 2.25. Network damage state depending on the damage state of the component

The earthquake catalog created in Section 2.3 give rise to 732 earthquake events in 10,000 years. The 732 earthquake events, characterized uniquely by the magnitude and the location of the event, give rise to a distribution of ground motion intensity measure (IM) as computed in Section 2.4. As previously mentioned, the peak ground acceleration (PGA) has been adopted as the IM for the fragility curve. The median PGA at each site for all the seismic scenario is used to compute the probability of being in each damage state from the fragility curve presented in Figure 2.23. Random scenarios are then created for each of the seismic events to estimate the damage state of each of the bridges and eventually the damage state of the highway network. Out of the 732 seismic events, 668 events have caused more than slight damage in the network which implies that at least one bridge in the network has structural damage and the network is disrupted for more than day. 56 events did not cause any damage to the network and 8 events give rise to

scenarios with a network in slight damage. This work is limited to look at the impacts of these 8 events. The portion of events causing the three different damage states in the network is shown in Figure 2.26:

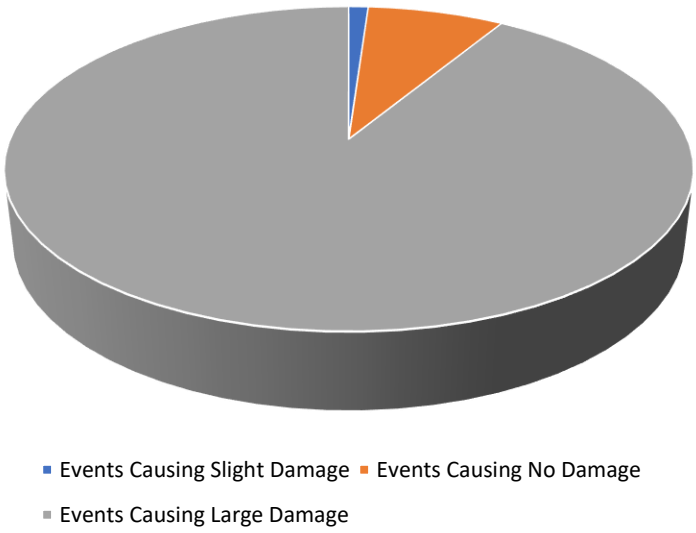

Figure 2.26. Distribution of Events based on its severity

The distribution of the events causing different levels of damage across the 26 rupture scenarios is presented in figure 2.27:

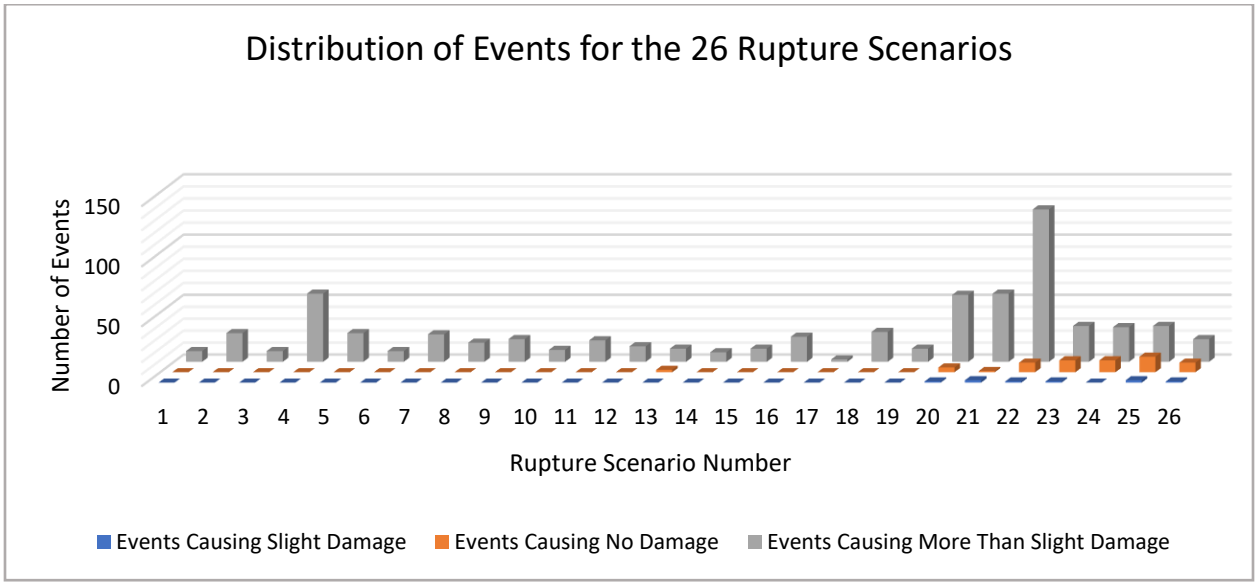

Figure 2.27. Distribution of Events Across the Rupture Scenarios

CHAPTER 3

DOWNTIME IN THE TRANSPORTATION NETWORK

3.1. Transportation Network & Traffic Data

The highway network considered for analysis is a section of the SR-91 which runs through Los Angeles, Orange and Riverside counties. This corridor of SR-91 passes through Anaheim, Fullerton, Placentia, and Yorba Linda and includes four major freeway-to-freeway interchanges: I-5, SR-57, SR-55, and the SR-241 Eastern Transportation Corridor Toll Road [CSMP SR-91, 2010]. This corridor of SR-91 is comprised of six to eight lanes in most of the network and also has auxiliary sections in some part of it. One High Occupancy Vehicle (HOV) runs through both ways of the corridor which allows vehicles with occupancy of more than two can ply 24 hours of the day, every day. The Caltrans traffic volume reported in 2008 that this corridor of SR-91 carries between 217,000 and 318,000 annual average daily traffic. SR-91 also carries large trucks and according to 2008 truck volumes from Caltrans, there is 4.5-8.7 percent of truck traffic along this corridor.

Figure 3.1. The SR-91 corridor (Source: Google Map)

All the traffic data required to conduct this traffic simulation has been taken from the Corridor System Management Plan survey carried out by System Metrics Group, Inc. in association with CLR Analytics, Inc. for Caltrans. Orange County Transportation Authority's (OCTA) travel demand model was relied on for analyzing the origins and destinations of the SR-91 corridor. The origin and destination are first identified by segregating the surrounding region by seven Traffic Analysis Zone (TAZ). The distribution of the seven TAZ has been shown in figure 3.2. The aggregated analysis zones are specific to

the CSMP study carried by the agencies mentioned above. Using the TAZ, the traffic demand is estimated in the SR-91 corridor for peak time during the day time. The time duration considered for estimating the traffic demand is 6 AM to 10 AM. The peak origin destination demand during the peak time of the day is presented in Table 3.2. The traffic demand pattern shows that 33% of the trips start and terminate inside Orange County, 27% of the trips originate inside Orange County but terminate outside, 32% of the trips start outside Orange County but end inside and 8% of the trips start and terminate outside Orange County. [CSMP Report, 2010].

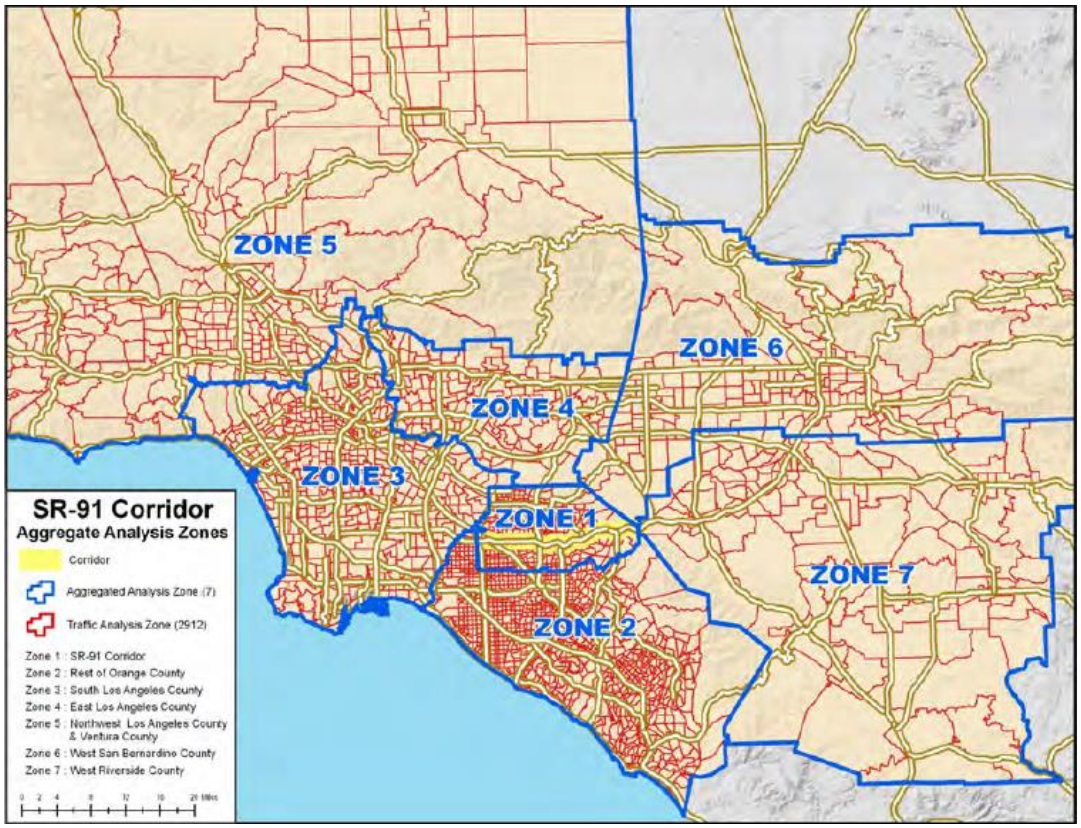

Figure 3.2. Traffic Analysis Zone (TAZ) profile for Traffic Demand Data
(Source: CSMP SR-91 Orange County Corridor Report, 2010)

Table 3.1. Traffic Demand Data for seven TAZ (Source: CSMP Report, 2010)

		Origin TAZ							
Destination TAZ	Day Trips	SR-91 Corridor	Rest of Orange County	South Los Angeles	East Los Angeles	NW Los Angeles & Venture	West San Bernardino	West Riverside	Outside Zone
	SR-91 Corridor	8743	20846	9870	1832	1231	2419	1356	286
	Rest of Orange County	33459	10379	35067	3375	3287	5531	7382	108
	South Los Angeles	9700	24132	5955	545	1210	790	1279	431
	East Los Angeles	2375	4026	820	1	139	0	182	91
	NW Los Angeles & Venture	1259	2785	1317	185	610	276	265	54
	West San Bernardino	2543	6207	965	1	183	1	254	111
	West Riverside	2550	4805	1338	140	278	209	295	88
	Outside Zone	154	48	157	26	35	32	32	1

The CSMP survey team analyzed the quality of the data used in the traffic demand analysis. This is important to ensure the reliability of the automatic sensor data. The available data for the analysis of SR-91 CSMP includes the following sources [CSMP Report, 2010]:

I. Caltrans Statewide Highway Congestion Monitoring Program (HICOMP) annual report and data files (2004-2007)

II. Caltrans Freeway detector data

III. Caltrans District 12 probe vehicle runs (electronic tachometer runs)

IV. Caltrans Traffic Accident Surveillance and Analysis System (TASAS)

V. Signal Timing Plans from the Cities of Anaheim, Fullerton and Yorba Linda

VI. Traffic study reports (various)

VII. Aerial photographs (Google Earth) and Caltrans photologs

VIII. Online Resources (i.e., OCTA website, Metrolink website, SCAG website, etc.)

3.2. Traffic Simulation with TransModeler

Traffic simulation was carried out in micro simulation software TransModeler to estimate the downtime in the highway network. The micro simulation model of the corridor of the SR-91 was created by the CLR-Analytics team for the CSMP survey. Micro simulation software are computationally intensive and it is very complex to model and calibrate traffic for a vast urban area such as the SR-91 corridor. Although it gives very reasonable estimation of the delay occurring in the networking and therefore a realistic quantification of the parameters is possible. Figure 3.3. shows the TransModeler model for the SR-91 corridor. The freeway interchanges along with the on-ramps and off-ramps were modeled. The model was calibrated with the actual 2007 model for traffic demand created by the survey team for the CSMP survey.

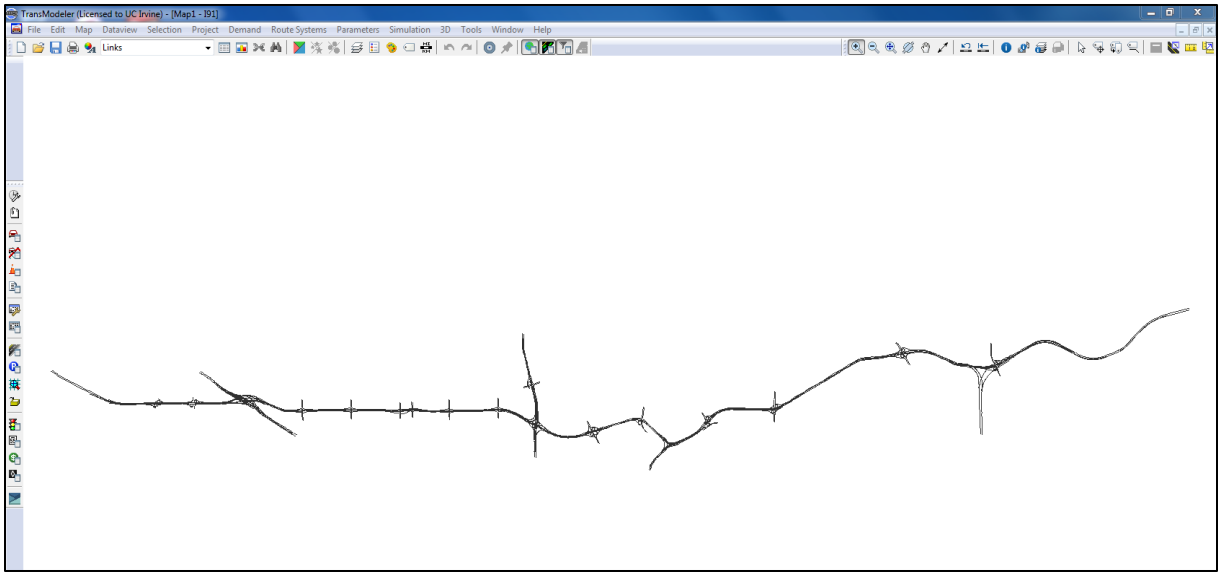

Figure 3.3. Model of SR-91 Corridor in TransModeler

The following techniques were used for the traffic simulation carried out for different scenarios of bridge disruption due to seismic events,

I. **Traffic Demand:** Traffic demand in TransModeler can be specified through a variety of methods, such as defining link volumes and turning movements, origin-destination trip tables, or a specific set of vehicle paths. The magnitude and the dynamics of the traffic should be defined to gather

accurate information from the simulation. Here, origin-destination trip tables are used to define the traffic demand. As previously mentioned, the simulation is run for the day time peak period of 4 hours, i.e. 6 AM to 10 AM. Four different origin-destination trip tables are used for every hour interval. The origin-destination trip tables compiled by the CSMP survey team has been used in this work.

II. **Warm-Up Period:** A warm up period of 10 min was implemented in the traffic simulation in TransModeler. The warm up period is provided in TransModeler to load the empty network. The TranModeler guide defines the simulation warm-up period as "When starting with an empty network, that length of time at beginning of each run that is dedicated to loading the network, not for deriving meaningful statistics". Therefore, the warm-up period helps to start the simulation with a meaningful traffic volume in the network, rather than starting with an empty network. This helps in a realistic realization of simulation outputs although the warm-period in the simulation is not used for deriving statistics of traffic performance.

III. **Route Choice:** TransModeler provides a selection for route choice in the network to calculate the paths of the trips. Route choice is complex decision and depends on driver behavior. As mentioned earlier, TransModeler is a path-based simulation model and therefore an assigned path to a trip is crucial. The pre-assigned path of a trip is referred to as *habitual path*, as most of the drivers tend to follow that path because of familiarity and as a routine decision out of habit. However, when an exceptionally high congestion occurs en-route or the driver experiences high amount of delay in the habitual path, the driver may consider alternate paths. Although, a section of the drivers would still be continuing in the same path because of habitual reasons and less impulsive personalities. The alternate route that a driver may choose in the event of unexpected delay and high congestion is determined by the route choice method. In this work, probabilistic route choice method is implemented. This method uses a multinormal logit model (MNL) choice model to simulate a driver's choice among a set of alternative paths, each having a utility that describes its relative attractiveness. The model then determines the probability of the driver choosing each of the paths.

Therefore, this model gives a realistic realization of the route choice behavior of driver when there is a disruption of traffic in the bridges due to seismic excitation.

IV. **Bridge Disruption:** To model the bridge disruption because of moderate damage state caused by seismic events, incidents are created at the particular location to block the traffic. Due to this, the traffic flow is interrupted and there is an exceptionally high congestion in the network. Therefore the incoming drivers would consider rerouting and as mentioned earlier would choose a better route provided by the probabilistic route choice method. This creates delays in the network and provides a parameter to quantify the downtime caused by the seismic event. To model the incidents in TransModeler, the starting time of the incident, duration of the incident, visibility and the capacity reduction is defined. The starting time and durations are defined as different combinations to come up with as many scenarios as possible. Also, 100% capacity reduction is modeled in the bridge sites so that the bridges are completely closed during the inspection process of the bridges following the seismic event.

3.3. Traffic Simulation Scenarios

The analysis carried out in section 2.5 gives rise to 8 scenarios where traffic simulation has to be carried out to estimate the delay in travel time due to the disruption of the bridges. The duration of bridge disruption due to non-structural damage cannot be explicitly correlated. MCEER report on Post-Earthquake Bridge Inspection Guideline (O'Connor et al., 2010) walks through the inspection procedure of the bridge inspection following an earthquake and specific roles of the residency staff, Resident Engineers (RE) and Regional Structures Engineer (RSE). Following a seismic event the residency staff carries out a preliminary drive in survey and barricades the damaged bridges. They report their observations to the RE. RSE oversee damage assessments based on the information gathered following the earthquake. But the duration of bridge disruption for non-structural damage and inspection of bridges are unavailable. Therefore, we consider two time duration for bridge closure, i.e. half hour and two hour closure for bridges corresponding to slight damage states. The half hour delay is possible in the case when there is a displacement of non-structural

component such as barrier rails and light poles which can be taken care of quickly by the resident staff to facilitate smooth flow of traffic. The two-hour closure of bridge can be attributed to a case when the residency staff barricades a bridge but the Resident Engineer clears it after inspection citing no serious damage to stall the traffic.

With these assumptions, the traffic simulations were run for each of the 8 scenarios of network disruption for half-hour and two-hour closure starting at 6 AM, 7AM, 8AM and 9AM. As the traffic data for the day time peak hours are available for conducting the traffic simulations we use a factor of 4 to convert the four-hour peak time delay to a daily delay [Moore et al., 2006].

The 8 bridge disruption scenarios created in Section 2.5 has different combination of the bridges being effected to be closed for either a half hour or two-hour duration. Out of the 8 scenarios, in 5 scenarios only one bridge in the network gets effected for a short shut down. On the other hand, in 1 scenario each two, three, and four bridges in the network have been closed. The different scenarios give rise to different nature of the traffic behavior during its closure and therefore different delay profiles were observed in each of the scenarios.

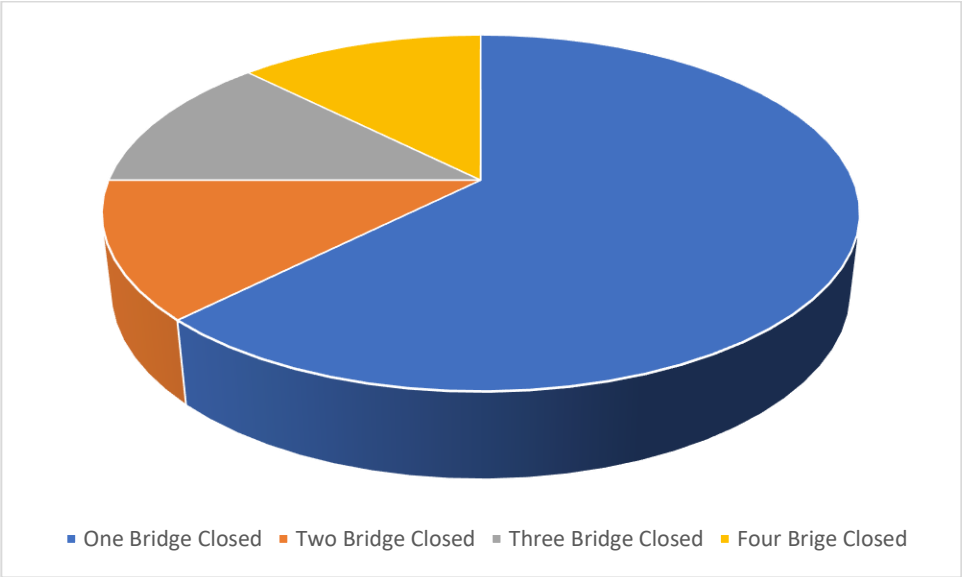

Figure 3.4. Distribution of Events based on the No of Bridges Affected

3.4. Economical Loss for Seismic Events

The performance of a highway network is gauged by the driver's delay due to congestion and trip opportunity loss due to reduction in opportunity [Nifuku and Shinozuka, 2014]. The accumulation of these losses is termed as social loss occurred due to seismic events. As the closure time is very less in the scenarios considered for this work, the trip reduction is very less (<1%). Hence the opportunity loss is neglected and the driver's delay has been adopted as the parameter to quantify the downtime of the highway network. The congestion in the highway network can be represented by the delay in travel time occurred during the disruption in the bridges. The delay is estimated by running the traffic simulations in TransModeler as described in the previous section and it is represented in hours. The delay is then converted to monetary loss by using driver time value estimated by Caltrans.

The Life-Cycle-Benefit-Cost analysis economic parameters computed by Caltrans are as given below:

Table 3.2. Life-Cycle-Benefit-Cost Analysis Economic Parameters (Source: Caltrans)

Value of Time	Dollar Per Person Hours
Automobile	US$ 12.50
Truck	US$ 28.70
Auto/Truck Composite (weighted average)	US$ 17.35
Average Vehicle Occupancy Rate	1.15

As discussed in the previous sections, the scenarios for quantifying the loss do not have any structural damage in the bridges of the network. Hence, there is no cost associated with the repair which is the direct loss. Therefore, the total loss occurred in the network in the considered scenarios are only the indirect loss or the social loss.

As discussed in Section 3.3. each of the 8 traffic scenarios have been simulated eight times for bridge closure of half-hour and two-hour duration starting from 6 AM, 7AM, 8AM and 9AM. Therefore, for each

of the scenarios there are eight corresponding loss amounts. The economic loss amounts in these scenarios for different time durations are presented in Figure 3.5

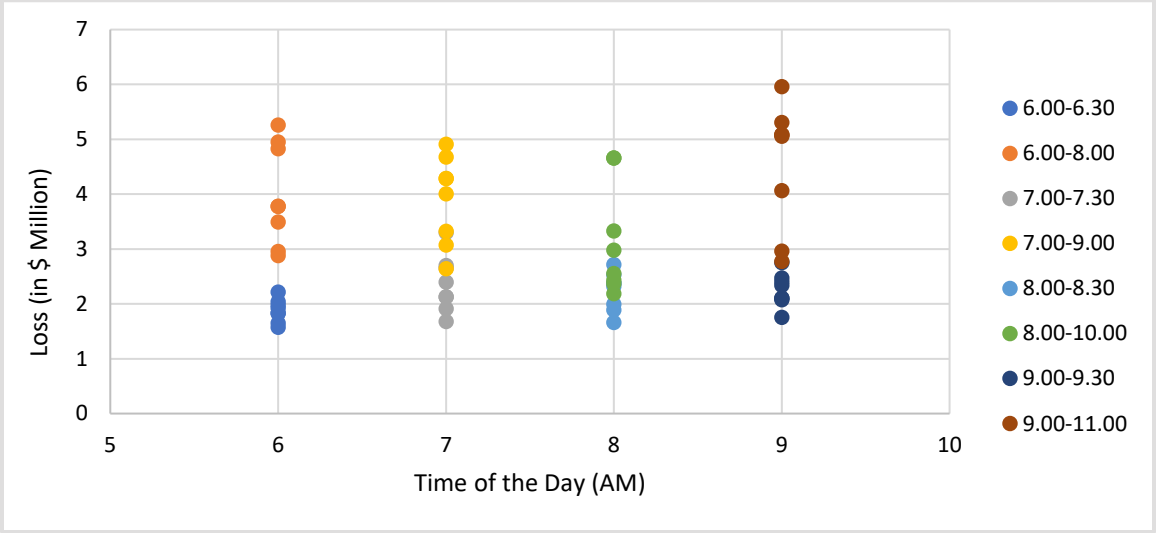

Figure 3.5. Daily Economic Loss due to the Disruption in the Network at Different Time of the Day during the Peak Time

The distribution of the economic loss at different time of the day and for different duration is presented in the following plots indicating the mean economic loss at each scenario and corresponding standard deviation.

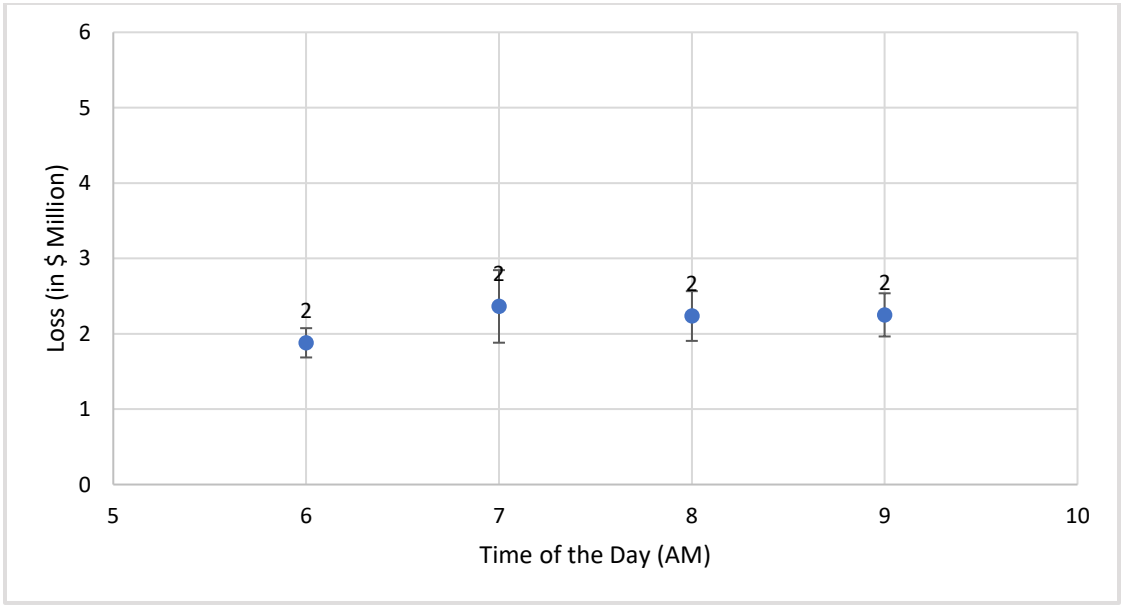

Figure 3.6. Mean and Standard Deviation of Loss due to Half an Hour Disruption

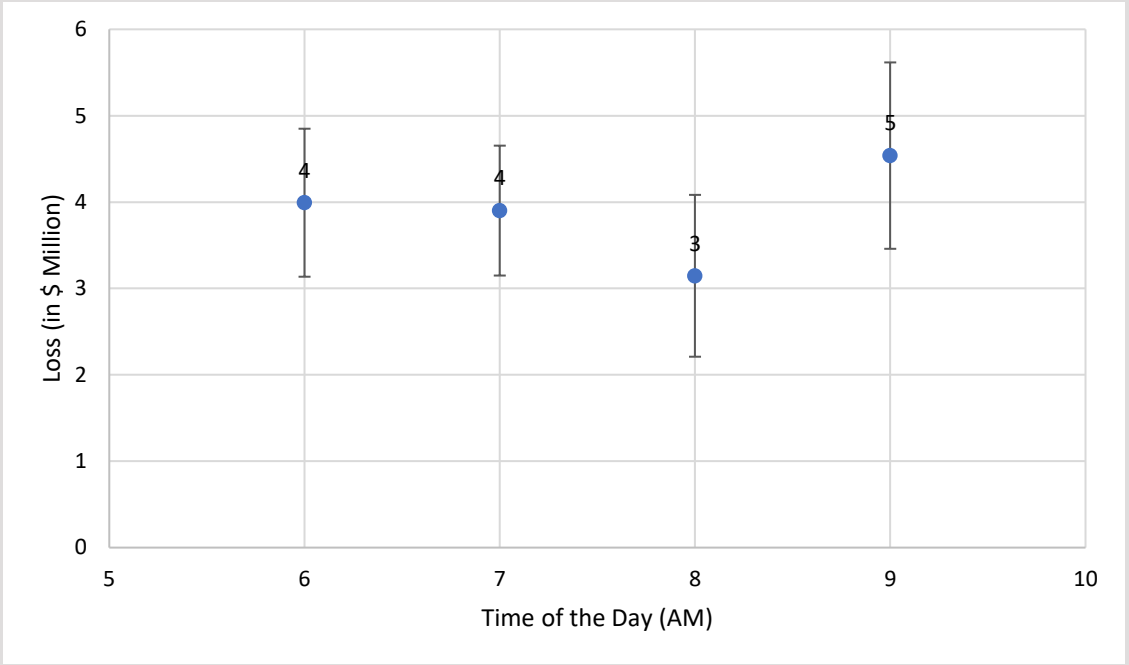

Figure 3.7. Mean and Standard Deviation of Loss due to Two Hour Disruption

As stated before in this section, 56 events did not cause any damage to the network whereas 668 events caused more than slight damage. Evidently, the 56 events not causing any damage did not incur any economic loss due to the seismic events. The economic loss due to these 668 events is not estimated in this work to concentrate on the small duration disruptions. As the information regarding these high amount loss is not computed in this scope of work, therefore a comprehensive mean annual rate of exceedance curve for economic losses cannot be estimated. Hence, a mean annual rate of exceedance curve for the economic losses due to short closure of bridges is evaluated, which in fact is a portion of the overall curve. This is presented in Figure 3.8.

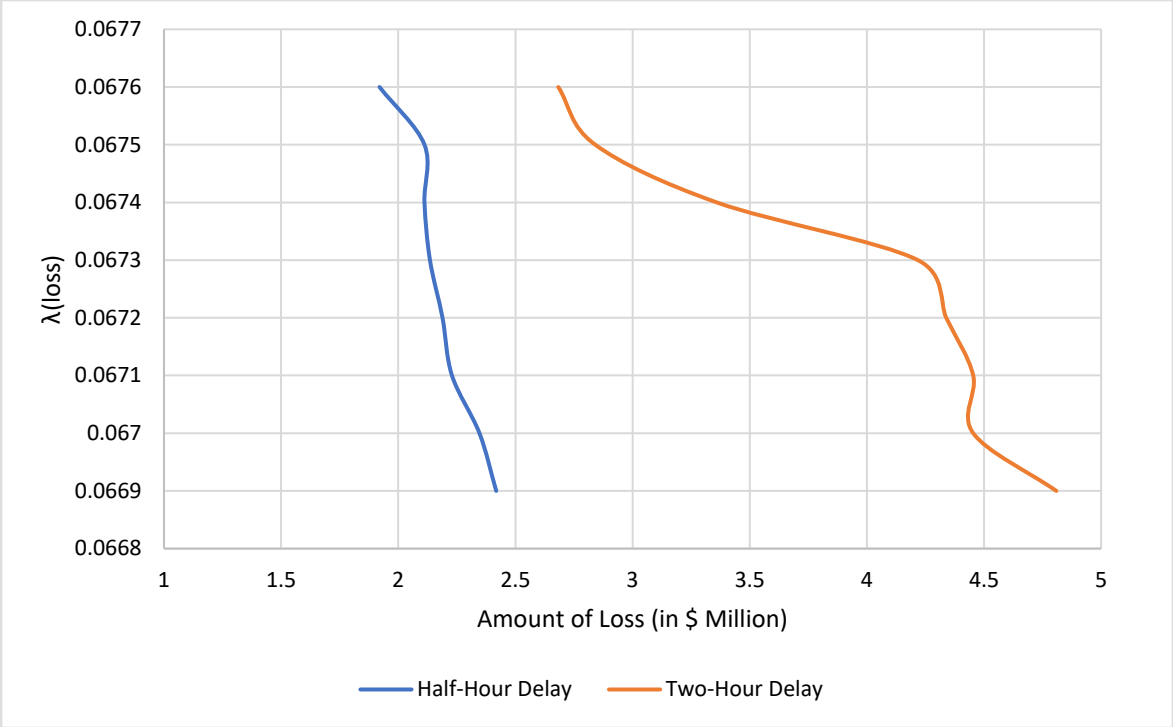

Figure 3.8. Mean Annual Rate of Exceedance of Loss

CHAPTER 4
CONCLUSION

4.1. Quantification of Downtime

This work focuses on quantifying the downtime of a highway network due to small and moderate ground motions which do not cause any structural damage in terms of the economic losses that it incurs. A methodology to quantify the downtime for these scenarios has been laid down with rigorous probabilistic seismic hazard analysis and traffic simulation techniques. The results presented in Section 2.3 shows that even short duration of disruption in the bridges give rise to losses in the order of $4 million. In Figure 3.6 it can be seen that the mean economic loss due to half hour disruption at different times of the day lies between $1.88 million to $2.36 million with a very small standard deviation. Whereas, for a two-hour disruption of bridges in the network, the mean economic loss, from figure 3.7 lies between $3.14 million to $4.53 million with a relatively higher standard deviation. From figure 3.8, it can be seen that social economic loss in the range of $2 million to $4 million due to short disruption of bridges in a highway network has an annual rate (λ_{loss}) of approximately 0.0675. This indicate that a social economic loss in the range of $2 million to $4 million will recur in every 15 years.

This information can be useful for agencies working towards a resilient infrastructure systems and make informed decision post an earthquake to mitigate the risk effectively to plan smart devices to monitor the performance of the bridges. The informed decision through smart devices regarding the closure of a bridge following an earthquake can reduce the duration of bridge closure. This eventually will help in saving an enormous amount of money.

4.2. Future Work:

As the work is focused on quantifying the loss for small to moderate level of ground shaking, it will be valuable to consider the small and medium sized seismic faults which produces small to moderate

earthquake events. Moreover, adopting a composite model for earthquake will capture many small earthquakes which can possibly create scenarios where there is short duration bridge closure. A similar methodology followed in this work can be carried out including the above factors to estimate the economic loss. Moreover, an updated traffic data and a comprehensive way of carrying out traffic simulation for longer durations can be considered to better the work.

REFERENCES

1. Bruneau, Michel, et al. "A framework to quantitatively assess and enhance the seismic resilience of communities." *Earthquake spectra* 19.4 (2003): 733-752.
2. Werner, Stuart D., et al. "A risk-based methodology for assessing the seismic performance of highway systems." (2000).
3. Banerjee, Swagata, and Masanobu Shinozuka. "Mechanistic quantification of RC bridge damage states under earthquake through fragility analysis." *Probabilistic Engineering Mechanics* 23.1 (2008): 12-22.
4. Jayaram, Nirmal, and Jack W. Baker. "Efficient sampling and data reduction techniques for probabilistic seismic lifeline risk assessment." *Earthquake Engineering & Structural Dynamics* 39.10 (2010): 1109-1131.
5. Werner, Stuart D., et al. *Redars 2 Methodology and software for seismic risk analysis of highway systems*. No. MCEER-06-SP08. 2006.
6. Cornell, C. Allin, and Helmut Krawlinker. “Progress and Challenges in Seismic Performance Assessment”. (2000)
7. Deierlein, Gregory G. "Overview of a comprehensive framework for earthquake performance assessment." *Performance-Based Seismic Design Concepts and Implementation, Proceedings of an International Workshop*. 2004.
8. Chang, Stephanie E., Masanobu Shinozuka, and James E. Moore. "Probabilistic earthquake scenarios: extending risk analysis methodologies to spatially distributed systems." *Earthquake Spectra* 16.3 (2000): 557-572.
9. Werner, Stuart D., et al. "New developments in seismic risk analysis of highway systems." *Research progress and accomplishments 2003–2004* (2004): 221-238.
10. Calvi, G. Michele, et al. "Development of seismic vulnerability assessment methodologies over the past 30 years." *ISET journal of Earthquake Technology* 43.3 (2006): 75-104.

11. Rose, Adam, et al. "Benefit-cost analysis of FEMA hazard mitigation grants." *Natural hazards review* 8.4 (2007): 97-111.
12. Corridor System Management Plan (CSMP), Orange County SR-91 corridor Final Report, 2010.
13. Krawinkler, Helmut, and Eduardo Miranda. "Performance-based earthquake engineering." *Earthquake engineering: from engineering seismology to performance-based engineering*. CRC Press, 2004.
14. Baker, Jack W., and C. Allin Cornell. *Uncertainty specification and propagation for loss estimation using FOSM method*. Pacific Earthquake Engineering Research Center, College of Engineering, University of California, 2003.
15. Comerio, Mary C. "Public policy for reducing earthquake risks: a US perspective." *Building Research & Information* 32.5 (2004): 403-413.
16. Porter, Keith A., James L. Beck, and Rustem Shaikhutdinov. "Simplified estimation of economic seismic risk for buildings." *Earthquake Spectra* 20.4 (2004): 1239-1263.
17. Gutenberg, Beno, and Carl F. Richter. "Earthquake magnitude, intensity, energy, and acceleration (second paper)." *Bulletin of the seismological society of America* 46.2 (1956): 105-145.
18. Youngs, Robert R., and Kevin J. Coppersmith. "Implications of fault slip rates and earthquake recurrence models to probabilistic seismic hazard estimates." *Bulletin of the Seismological society of America* 75.4 (1985): 939-964.
19. Wells, Donald L., and Kevin J. Coppersmith. "New empirical relationships among magnitude, rupture length, rupture width, rupture area, and surface displacement." *Bulletin of the seismological Society of America* 84.4 (1994): 974-1002.
20. Idriss, I. M. *Procedures for Selecting Earthquake Ground Motions at Rock Sites*. US Department of Commerce, National Institute of Standards and Technology, 1993.
21. Sadigh, K., et al. "Attenuation relationships for shallow crustal earthquakes based on California strong motion data." *Seismological research letters* 68.1 (1997): 180-189.Sadigh et al., (1997);

22. Campbell, Kenneth W. "Empirical near-source attenuation relationships for horizontal and vertical components of peak ground acceleration, peak ground velocity, and pseudo-absolute acceleration response spectra." *Seismological Research Letters* 68.1 (1997): 154-179.
23. Bozorgnia, Yousef, Kenneth W. Campbell, and Mansour Niazi. "Observed spectral characteristics of vertical ground motion recorded during worldwide earthquakes from 1957 to 1995." *Proceedings of the 12th world conference on earthquake engineering*. Vol. 2671. No. 4. New Zealand:[sn], 2000.
24. Atkinson, Gail M., and David M. Boore. "Stochastic point-source modeling of ground motions in the Cascadia region." *Seismological Research Letters* 68.1 (1997): 74-85.
25. Working Group on California Earthquake Probabilities, Earthquake Probabilities in the San Francisco Bay Region: 2002-2031, USGS, (2003)
26. Boore, David M. "Simulation of ground motion using the stochastic method." *Seismic Motion, Lithospheric Structures, Earthquake and Volcanic Sources: The Keiiti Aki Volume*. Birkhäuser Basel, 2003. 635-676.
27. Dabaghi, Mayssa. "Stochastic modeling and simulation of near-fault ground motions for performance-based earthquake engineering." (2014).
28. King S., Kiremidjian A., Pachakis D. and Sarabandi P., "Application of Empirical Fragility Functions from Recent Earthquakes," *Proceedings of the 13th World Conference on Earthquake Engineering, Vancouver, BC, Canada. Paper No. 2829, (2004)*
29. Lee, Jian-Cheng, et al. "Geometry and structure of northern surface ruptures of the 1999 Mw= 7.6 Chi-Chi Taiwan earthquake: influence from inherited fold belt structures." *Journal of Structural Geology* 24.1 (2002): 173-192.
30. Eguchi, Ronald T., et al. "Resilient disaster response: using remote sensing technologies for post-earthquake damage detection." *Research Progress and Accomplishments: 2001-2003* (2003): 125-137.

31. Padgett, Jamie E., and Reginald DesRoches. "Bridge functionality relationships for improved seismic risk assessment of transportation networks." *Earthquake Spectra* 23.1 (2007): 115-130.
32. Moore, James E, et al. “Quantifying Economic Losses from Travel Forgone Following a Large Metropolitan Earthquake.” (2006).
33. O’Connor, Jerome S., et al. “Post-Earthquake Bridge Inspection Guidelines.” (2010)
34. Cramer, Chris H., and Mark D. Petersen. "Predominant seismic source distance and magnitude maps for Los Angeles, Orange, and Ventura counties, California." *Bulletin of the Seismological Society of America* 86.5 (1996): 1645-1649.
35. Hanks, Thomas C., and William H. Bakun. "M-logA observations for recent large earthquakes." *Bulletin of the Seismological Society of America* 98.1 (2008): 490-494.
36. Aki (1997)
37. Hancock, Jonathan, et al. "An improved method of matching response spectra of recorded earthquake ground motion using wavelets." *Journal of earthquake engineering* 10.spec01 (2006): 67-89.
38. Yamamoto, Yoshifumi, and Jack W. Baker. "Stochastic model for earthquake ground motion using wavelet packets." *Bulletin of the Seismological Society of America* 103.6 (2013): 3044-3056.
39. Campbell, Kenneth W., and Yousef Bozorgnia. "NGA-West2 ground motion model for the average horizontal components of PGA, PGV, and 5% damped linear acceleration response spectra." *Earthquake Spectra* 30.3 (2014): 1087-1115.
40. Hwang, Howard, John B. Jernigan, and Yang-Wei Lin. "Evaluation of seismic damage to Memphis bridges and highway systems." *Journal of Bridge Engineering* 5.4 (2000): 322-330.
41. Shinozuka, Masanobu, et al. "Effect of seismic retrofit of bridges on transportation networks." *Earthquake Engineering and Engineering Vibration* 2.2 (2003): 169-179.
42. Choi, Eunsoo, Reginald DesRoches, and Bryant Nielson. "Seismic fragility of typical bridges in moderate seismic zones." *Engineering Structures* 26.2 (2004): 187-199.Mackie and Stojadinovic 2004

43. Nielson, Bryant G., and Reginald DesRoches. "Analytical seismic fragility curves for typical bridges in the central and southeastern United States." *Earthquake Spectra* 23.3 (2007): 615-633.
44. Zakeri, Behzad, and Gholamreza Ghodrati Amiri. "Probabilistic performance assessment of retrofitted skewed multi span continuous concrete I-girder bridges." *Journal of Earthquake Engineering* 18.6 (2014): 945-963.
45. Zakeri, Behzad and Farzin Zareian. “Bridge Design Framework for Target Seismic Loss.” *Journal of Bridge Engineering, In Press* (2017)